Efficiency Performance Optimization of Wireless Power Transfer System with Magnetic Resonance

Seunggyu Lee

Electrical Engineering Program

Graduate school of UNIST

2013

Efficiency Performance Optimization of Wireless Power Transfer System with Magnetic Resonance

Seunggyu Lee

Electrical Engineering Program

Graduate school of UNIST

Efficiency Performance Optimization of Wireless Power Transfer System with Magnetic Resonance

A thesis
submitted to the Graduate School of UNIST
in partial fulfillment of the
requirements for the degree of
Master of Science

Seunggyu Lee

2. 5. 2013
Approved by

Major Advisor
Franklin Bien

Efficiency Performance Optimization of Wireless Power Transfer System with Magnetic Resonance

Seunggyu Lee

This certifies that the thesis of Seunggyu Lee is approved.

2. 5. 2013

Thesis Supervisor: Franklin Bien

Jaejoon Kim: Thesis Committee Member #1

Jaehyouk Choi: Thesis Committee Member #2

Abstract

Wireless Power Transfer (WPT) system has attracted people's attention for a kind of power transfer mechanism. This technology provides energy to communication devices or electrical devices without the power connection. The concept of Wireless Power Transfer (WPT) can be traced back to the early 20th century when Nikola Tesla patented several techniques related to transmitting power over air. However, there was not demanded due to the lack of portable electrical devices. Recently, the usage of mobile devices such as cell phones, PDAs, laptops, tablets, and other handheld gadgets equipped with rechargeable batteries has been widely spreading. That's why this technology has been attracting a lot of attention of scientists and R&D firms around the world to remove recharge cables. Wireless Power Transfer (WPT) system supports the usability to supply power for electrical devices without any connecting to power source directly.

The point of requirement of the applications using Wireless Power Transfer (WPT) system is transfer efficiency for reducing energy loss. Also, resonator size is important factor to apply real applications. In this thesis, technology to improve the system performance of Wireless Power Transfer (WPT) in magnetic resonance based scheme is described. Also, optimal efficiency conditions are derived and used to design optimal adaptive matching technique.

Contents

List of Figures

(C) S21 with axial-misalignment and without matching.

(D) S11 with axial-misalignment and without matching.

(E) S21 with axial-misalignment and matching.

(F) S11 with axial-misalignment and matching.

List of Tables

Nomenclature

AC Alternating Current.

ADS Advanced Design System.

EM Electromagnetic.

HFSS High Frequency Structure Simulator.

KVL Kirchhoff’s Voltage Law.

MIT Massachusetts Institute of Technology.

PA Power Amplifier.

R&D Research & Development.

UHF Ultra High Frequency.

VHF Very High Frequency.

VNA Vector Network Analyzer.

WPT Wireless Power Transfer.

Chapter I

Introduction

The history of the wireless power transfer technology date back to the late of 19th century with derivation that energy could be propagated from one point to other point in the free space from Maxwell in his writing “Treatise on Electricity and Magnetism” [1]. Over time, Nikola Tesla’s experiments are often considered as being some of the most salient works of the possibility of transmitting power through air. The successful realization of the wireless power transfer is required more specific analysis and is needed innovative solutions.

This chapter provides fundamental analysis of wireless power transfer such as definition of the wireless power transfer, classification, and essential parameters. As a result, the contribution points for wireless power transfer system in this thesis are stated.

1.1 Motivation and related works

Wireless power transfer (WPT) is a breakthrough technology that provides energy to communication devices without the power units. With the remarkable progress being made recently, this technology has been attracting a lot of attention of scientists and R&D firms around the world. The concept of WPT traces back to the 19th century when means of transmitting electrical power wirelessly was being researched.

As early 20th century, Nikola Tesla studied this phenomenon, patenting several techniques by which power could be transmitted [2], [3]. However, there was never strong demand for it due to the lack of portable consumer electronics devices.

Recently, the usage of mobile appliances such as cellphones, PDAs, laptops, tablets, and other handheld gadgets, equipped with rechargeable batteries has been widely spreading. Even though there have been several techniques to reduce the power consumption or improve battery life [4]. Most users are still required to manually connect their devices to wired charging systems every time the battery is low. Thus, the need for a technique to wirelessly charge these devices has re-emerged from such an inconvenience.

WPT technology not only helps reduce the cost of the devices but also significantly enable the portability and flexibility properties. Until now there have been many efforts to be made to improve

this technology as well as its applications. These efforts are able to be classified into three categories based on transmission range. Short range wireless power transfer indicates that the transmission distance is within several millimeters and typical representation of such transmission type is inductive wireless power transfer which is relied on the inductive coupling principle of a simple transformer [5]. Actually, inductive wireless power transfer is fit for short distance and very high power transfer wirelessly. Although the investigation of long range power delivery with microwaves was carried out with endeavors [6], the efficiency or power delivery is still quite low that is not sufficient to fully charge typical electronic gadgets overnight. In addition, when using these far-field techniques, any obstruction in the transfer path is not allowed. It is dangerous for human bodies or other organisms which in the energy transfer path according to IEEE standard for radio frequency electromagnetic fields [7]. Such power transfer are relatively suited to very low power applications unless they are used in military or space explorations which are less regulated environments.

In 2007, Professor Marin Soljacic and his team proposed the technique of the medium-range WPT relied on magnetic resonance [8] which has been a growing research area that finds wide applications these days. Comparing with previous wireless transmission technologies, magnetic resonance based wireless power transfer has some essential differences. Literally, the transmission range of magnetic resonance wireless power transfer is quite longer than that of inductive wireless power transfer which is able to transmit power within just several millimeters. Also, its transmission power level ranges from a few watts to several hundred watts as opposed to mm-watts level by microwaves.

Therefore, magnetic resonance based wireless power transfer technology is expected as a new technology of having.

1.2 Comparison of wireless power transfer technologies

As explained in previous section, wireless power transfer technology could be categorized according to transferred distance and mechanism. This section is described each technology as inductive wireless power transfer, capacitive wireless power transfer, magnetic resonance wireless power transfer, and microwave wireless power transfer.

1.2.1 Inductive and capacitive wireless power transfer

Inductive wireless power transfer technique is popular technology for transferring power wirelessly over a short range. This technique is very similar to transformer operation. And transferring power

could be derived by using *Ampere's law* and *Faraday's law*. The operation of inductive wireless power transfer is based on magnetic fields movement. Especially, current could generate magnetic field and magnetic field move from primary coil to alternative coil that could be established coil current. This technique is one of candidate for wirelessly transferring power through air and has easily found various applications such as consumer electronics, biomedical implants, mobile devices, and contactless gadgets. Hence it also have drawback that is limited transfer distance.

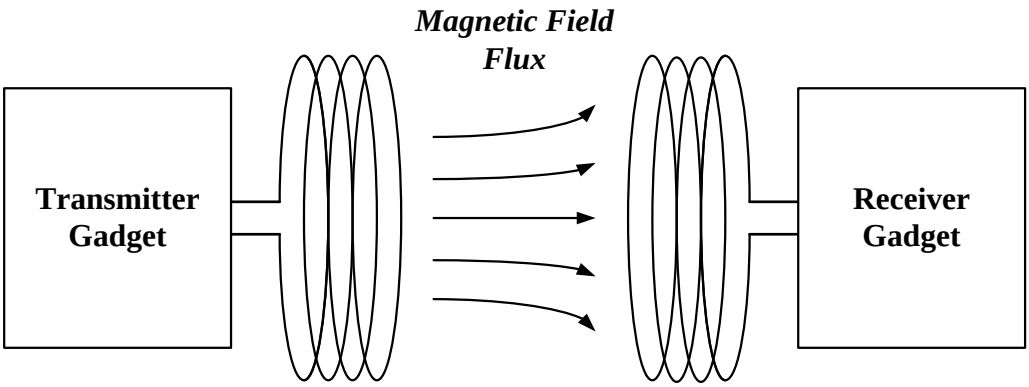

Figure 1-1: Conceptual diagram about inductive wireless power transfer.

Capacitive wireless power transfer is one of idea for substitution of inductive wireless power transfer technology. This technique is based on the AC power source is applied to the plates of the capacitor that are placed sufficiently close to each plate. From this condition, electric fields are formed between two plates and AC power could be passed through primary plate to secondary plate. In this case, if there are existed some other material between two plates, transfer power could be reduced.

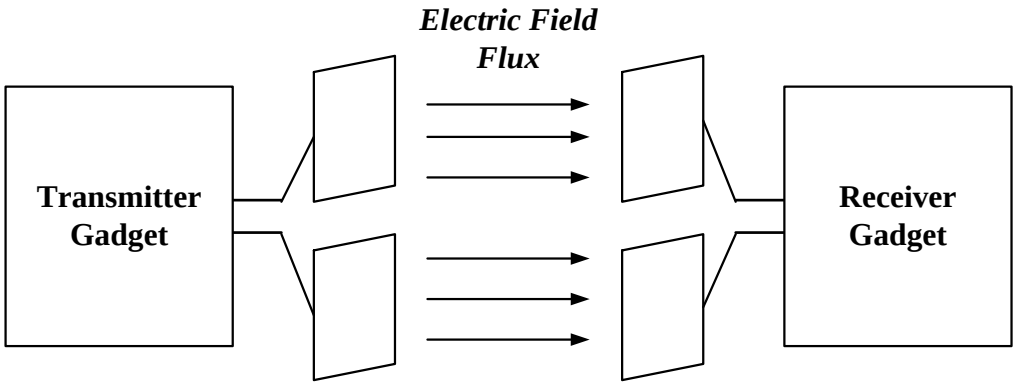

Figure 1-2: Conceptual diagram about capacitive wireless power transfer.

1.2.2 Magnetic resonance wireless power transfer

Magnetic resonance wireless power transfer is based on two self-resonant coils. And this scheme consists of four coils. Self-resonant coils could be represented the distributed inductance and distributed capacitance to achieve resonance. Power could be transferred each side from resonance phenomenon. Especially, magnetic resonance wireless power transfer has ability of mid-range power transfer wirelessly due to non-radiating mechanism. This works invented research group of MIT and they are successfully experimented wireless power transfer that received power more than 60W at 2m distance. So this technique is good candidate for wireless power transfer applications.

Figure 1-3: Magnetic resonance wireless power transfer.

1.2.3 Microwave wireless power transfer

Microwave wireless power transfer is used radio frequency wave that is electromagnetic wave. Many researchers used this technology to achieve long range and high power transfer wirelessly.

This technology has some advantages that are similar to RF communication system due to using high frequency and use conventional antenna such as patch antenna, Yagi-Uda antenna and horn antenna. But it also has drawback, transmitter and receiver always aligned to get higher efficiency and antenna needs higher directivity because RF wave has short wave length to move great distances.

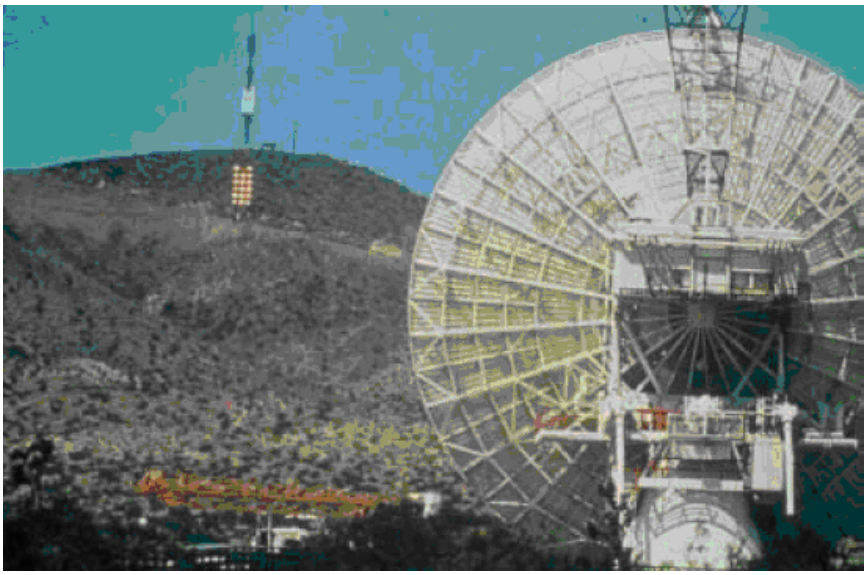

Figure 1-4: First Ground to Ground microwave wireless power transfer experiment in 1975 in [9].

1.3 Parameters for wireless power transfer system design

1.3.1 Mutual inductance

Closed form equations for the mutual inductance of two filamentary (electrically small, with wire radius $\ll$ coil radius) coils for all physical arrangements have been derived [10]-[12]. Figure 1-5 shows all relevant variables for calculations.

The relevant equations defining the mutual inductance between two such coils are as follows

$$M_{12} = \frac{2\mu_0}{\pi}\sqrt{r_1 r_2}\int_0^{\pi} \frac{\left[\cos\theta - \frac{c}{r_2}\cos\phi\right]\psi(k)}{k\sqrt{V^3}}d\phi \tag{1.1}$$

Where

$$\alpha = \frac{r_2}{r_1},\ \ \beta = \frac{d}{r_1}$$

$$V = \sqrt{1 - \cos^2\phi \sin^2\theta - 2\frac{c}{r_2}\cos\phi\cos\theta + \frac{c^2}{r_2^2}}$$

$$k^2 = \frac{4\alpha V}{\left(1+\alpha V\right)^2 + \xi^2},\ \ \xi = \beta - \alpha \cos\phi \sin\theta$$

$$\psi(k) = \left(1 - \frac{k^2}{2}\right) K(k) - E(k)$$

Where *K(k)* and *E(k)* are complete elliptic integrals of the first and second kind, respectively, as follows

$$K(k) = \int_0^{\frac{\pi}{2}} \frac{d\beta}{\sqrt{1 - k^2 \sin^2 \beta}} \tag{1.2}$$

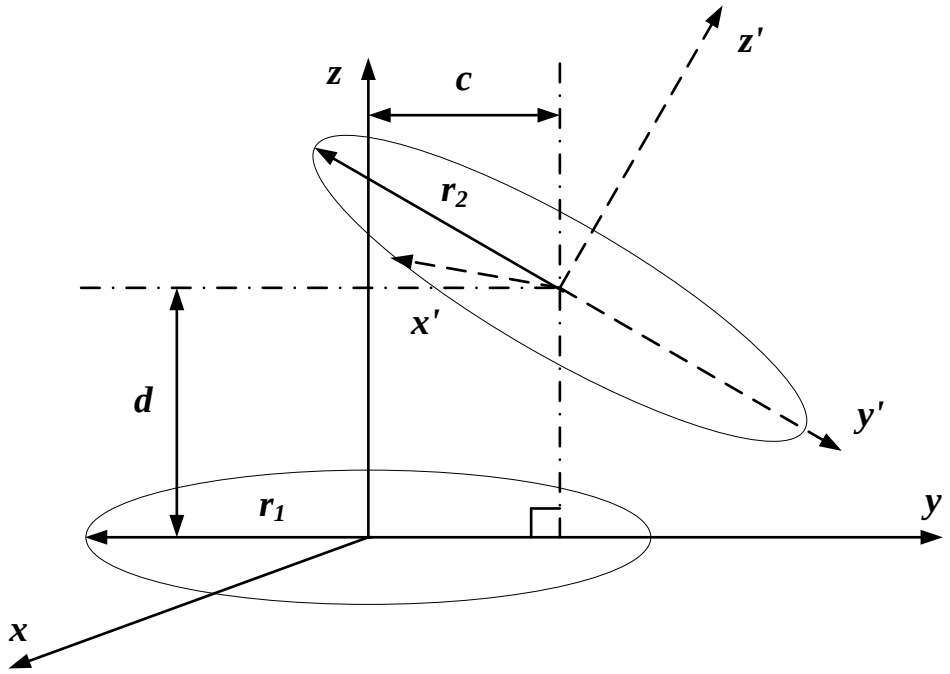

Figure 1-5: Two coils with variable defined for all positions.

$$E(k) = \int_0^{\frac{\pi}{2}} \sqrt{1 - k^2 \sin^2 \beta}\, d\beta \tag{1.3}$$

These equations define the mutual inductance between two coils for any configurations.

1.3.2 Simplified mutual inductance for aligned coils

The mutual inductance for two coils aligned co-axially (along the same central axis) as shown in

figure 1-6 reduces to a less complex equation. The mutual inductance was solved by application of Neumann's relations in [13]. Equation (1.1) reduces to

$$M_{12} = \mu\sqrt{r_1 r_2}\left[\left(\frac{2}{k} - k\right)K - \frac{2}{k}E\right] \tag{1.4}$$

Where

$$k^2 = \frac{4r_1 r_2}{\left(r_1 + r_2\right)^2 + d^2} \tag{1.5}$$

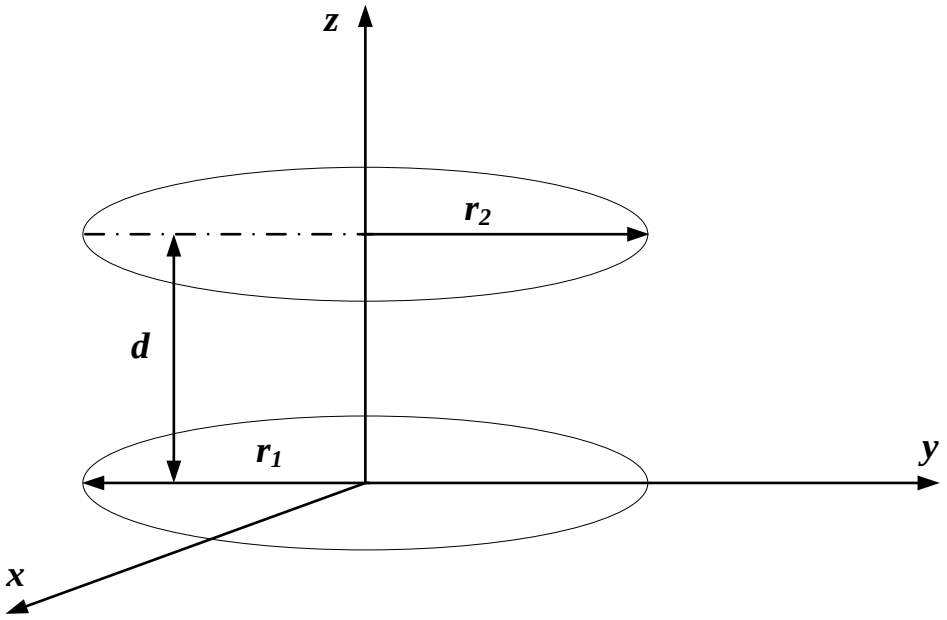

Figure 1-6: Two coils arranged co-axially along a central axis.

1.3.3 Coupling coefficient

Generally, the amount of inductive coupling that exists between the two coils is expressed as a fractional number between 0 and 1 instead of a percentage value, where 0 indicates zero or no inductive coupling, and 1 indicating full or maximum inductive coupling. In other words, if k =1 the two coils are perfectly coupled, if $k > 0.5$ the two coils are said to be tightly coupled and if $k < 0.5$ the two coils are said to be loosely coupled. Then the equation of mutual inductance which assumes a perfect coupling could be modified to take into account this coefficient of coupling, k and is given as

$$k = \frac{M}{\sqrt{L_1 L_2}} \tag{1.6}$$

When the coefficient of coupling, *k* is equal to 1, such that all the lines of flux of on coil cuts all of the turns of the other, the mutual inductance is equal to the geometric mean of the two individual inductances of the coils. So when the two inductances are equal and L_1 is equal to L_2, the mutual inductance that exists between the two coils could be defined as

$$M = \sqrt{L_1 L_2} = L \tag{1.7}$$

1.3.4 Resistance

For a coil with N turns and made of a material with conductivity σ, the modified standard formulas for ohmic (R_o) and radiation (R_r) resistances are given as below [8]

$$R_o = \sqrt{\frac{\mu_0 \omega}{2\sigma}} \frac{l}{4\pi a} \tag{1.8}$$

$$R_r = \sqrt{\frac{\mu_0}{\varepsilon_0}} \left[\frac{\pi}{12} N^2 \left(\frac{\omega R}{c} \right)^4 + \frac{2}{3\pi^3} \left(\frac{\omega h}{c} \right)^2 \right] \tag{1.9}$$

Where ω is angular frequency and *c* is represented speed of light.

The ohmic losses caused by the AC resistance from currents travelling on the outside of conductor. The skin depth is defined as δ = *sqrt(2/ωσμ)*, with σ = 5.96 x 10^7 for copper. For *f* >10 MHz, the skin depth is approximately 20 um.

1.4 Thesis contribution

This thesis concentrates on the aspects of theoretical verification and techniques to design efficiency enhancement of wireless power transfer system with magnetic resonance in the practical environment.

Circuit modeling and analysis of the magnetic resonance based wireless power transfer system help to understand more complicated cases, In reality, due to the resonant coupling nature of the system,

there is an optimum range between power coil and transmitting coil for a fixed distance between the transmitting and receiving coils. This phenomenon may not be clarified by a conventional magnetic theory.

In this thesis, an equivalent circuit model for magnetic resonance based wireless power transfer will be verified and analytically solved problem. In addition, techniques for improving efficiency of the wireless power transfer systems with changing coupling coefficient and misalignment condition will be proposed. Theoretical analysis are studied and compared with EM simulation and circuit verification by ADS, as well as experiments.

The practical contribution is aimed at those who involved in the field of wireless power transfer engineer, R&D firms, and students. This thesis is offering a new approach and focus that is not substantially found in other magnetic resonance based wireless power transfer studies.

Chapter II

Circuit Modeling and Analysis for Wireless Power Transfer System with Magnetic Resonance

This chapter demonstrates the circuit modeling and analysis of wireless power transfer system, and inspection about important factors. From this method, it is possible to understand various issues when magnetic resonance based wireless power transfer system are designed.

2.1 Modeling and analysis about resonator

The resonator of wireless power transfer could usually be modeled by series RLC lumped-element equivalent circuit, and it is possible to derive by using basic equations and circuits. The series RLC resonant circuit is described in figure 2-1.

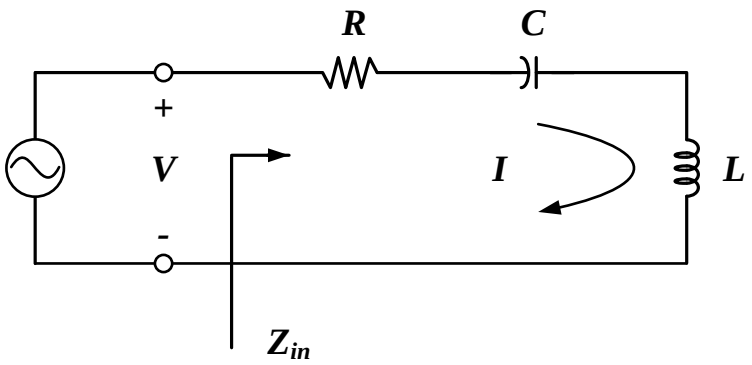

Figure 2-1: The series RLC circuit.

From figure 2-1, the series RLC resonant circuit has input impedance that is

$$Z_{in} = R + j\omega L - j\frac{1}{\omega C} \tag{2.1}$$

And the complex power delivered to the resonator is

$$P_{in} = \frac{1}{2}VI^{*} = \frac{1}{2}Z_{in}\left|I\right|^{2} = \frac{1}{2}Z_{in}\left|\frac{V}{Z_{in}}\right|^{2} = \frac{1}{2}\left|I\right|^{2}\left(R + j\omega L - j\frac{1}{\omega C}\right) \tag{2.2}$$

The power dissipated by the resistor, R, is

$$P_{loss} = \frac{1}{2}|I|^2 R \tag{2.3}$$

The average magnetic energy stored in the inductor, L, is

$$W_m = \frac{1}{4}|I|^2 L \tag{2.4}$$

And the average electric energy stored in the capacitor, C, is

$$W_e = \frac{1}{4}|V_C|^2 C = \frac{1}{4}|I|^2 \frac{1}{\omega^2 C} \tag{2.5}$$

Where V_c is the voltage across the capacitor. Then the complex power of equation (2.2) could be rewritten as (2.6).

$$P_{in} = P_{loss} + 2j\omega(W_m - W_e) \tag{2.6}$$

And the input impedance of (2.1) could be rearranged as (2.7).

$$Z_{in} = \frac{2P_{in}}{|I|^2} = \frac{P_{loss} + 2j\omega(W_m - W_e)}{\frac{1}{2}|I|^2} \tag{2.7}$$

Resonance basically occurs when the average stored magnetic and electric energies are equal, it means $W_m = W_e$. Then from (2.7) and (2.5), the input impedance at resonance is

$$Z_{in} = \frac{P_{loss}}{\frac{1}{2}|I|^2} = R \tag{2.8}$$

At this time, input impedance is purely real value. From equations (2.4) and (2.5), $W_m = W_e$ implies that the resonant frequency, ω_o, should be defined as (2.9)

$$\omega_o = \frac{1}{\sqrt{LC}} \tag{2.9}$$

To understand resonator for wireless power transfer system, quality factor is another important factor, Q which is defined as (2.10)

$$Q = \omega \frac{\left(\text{average energy stored}\right)}{\left(\text{energy loss/second}\right)} = \omega \frac{W_m + W_e}{P_{loss}} \tag{2.10}$$

Therefore quality factor could be measured loss of the resonant circuit. If the resonant circuit has lower loss, then it has higher quality factor. From the series type resonant circuit in figure 2-1, the Q could be calculated from (2.10) using equation (2.3), and assuming resonance that condition is $W_m = W_e$. It is possible to derive following.

$$Q = \omega_o \frac{2W_m}{P_{loss}} = \frac{\omega_o L}{R} = \frac{1}{\omega_o RC} \tag{2.11}$$

The quality factor, Q, could have a value between 0 and infinity. But it is difficult to obtain nearly infinity value. And if quality factor has higher value, this resonator has narrower bandwidth in the frequency domain. It means selectivity is goes up while in case of resonance frequency is changed from external effect. Power transfer efficiency is rapidly goes down.

2.2 Loaded, unloaded, external quality factor about resonator

The quality factor in the section of 2.1 is the characteristic of the resonant circuit without any loading effects caused by external elements. This quality factor is usually called the unloaded quality factor. In practice, however, a resonator is connected to matching circuit and other components, which will always have effect of lowering unloaded quality factor. It is called loaded Q, Q_L. In figure 2-2, this figure depicts a resonator connected to an external load resistor, R_L. Assuming the resonant circuit is a series RLC circuit, the load resistor R_L adds in series with R on the figure 2-1. Total resistance is $R + R_L$. From above assumption, external Q, Q_e, defined as

$$Q_e = \frac{\omega_o L}{R_L} \tag{2.12}$$

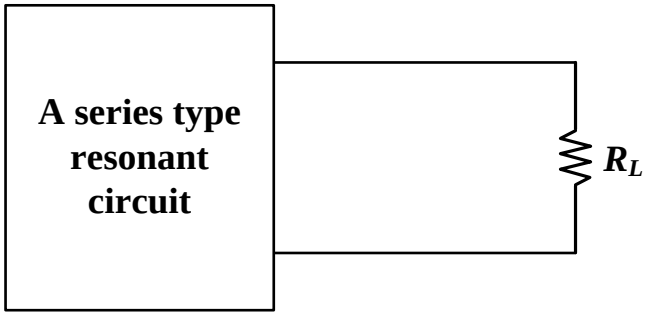

Figure 2-2: Configuration of a series type resonant circuit connected to load.

Then the loaded Q could be expressed as

$$\frac{1}{Q_L} = \frac{1}{Q_e} + \frac{1}{Q} \tag{2.13}$$

2.3 Circuit modeling about wireless power transfer system with magnetic resonance

The magnetic resonance based WPT techniques are typically based on four coils as opposed to two coils used in the conventional inductive links. A typical model of four-coil power transfer system is shown in figure 2-3, which consists of a power coil, a transmitting coil (Tx coil), a receiving coil (Rx coil) and a load coil. The Tx coil and Rx coil are so-called resonators, which are supposed to resonate at the same frequency. For common cases, four coils are different in size. Indeed, in some applications, the coils in the receiver side are needed to be scaled as small enough to be integrated in portable devices such as laptops, handheld devices or implantable medical equipment. In various cases of practical interest, the receiving and load coils can be fitted within the dimensions of those personal assistant tools, enabling mobility and flexibility properties. Otherwise, it is quite free to determine sizes of the transmitter. Normally, the transmitting coil can be made larger for the higher efficiency of the system. For the system in figure 2-3, a drawback of a low coupling coefficient between the Tx and Rx coils, as they locate a distance away from each other, is possibly overcome by using high-Q coils. This may help improve the system performance. In other words, the system is able to maintain the high efficiency even when the receiver moves far away from the transmitter. In the transmitting part, a signal generator is used to generate a sinusoidal signal oscillating at the frequency of interest. A power of the output signal from the generator is too small, approximately ten to hundreds of mm watts, to power devices of tens of watts. Hence, this signal is delivered to the Tx coil through a power amplifier (PA) for signal power amplification. In the receiver side, the receiving resonator and then load coil will transfer the induced energy to a connected load such as a certain electronic device. While the efficiency of the two-coil counterpart is not proportionally depending on the operating distance, the four-coil system is less sensitive to changes in the distance between the Tx and Rx coils. This kind of system can be optimized to provide a maximum efficiency at the given operating distance. These characteristics will be analyzed in the succeeding sections.

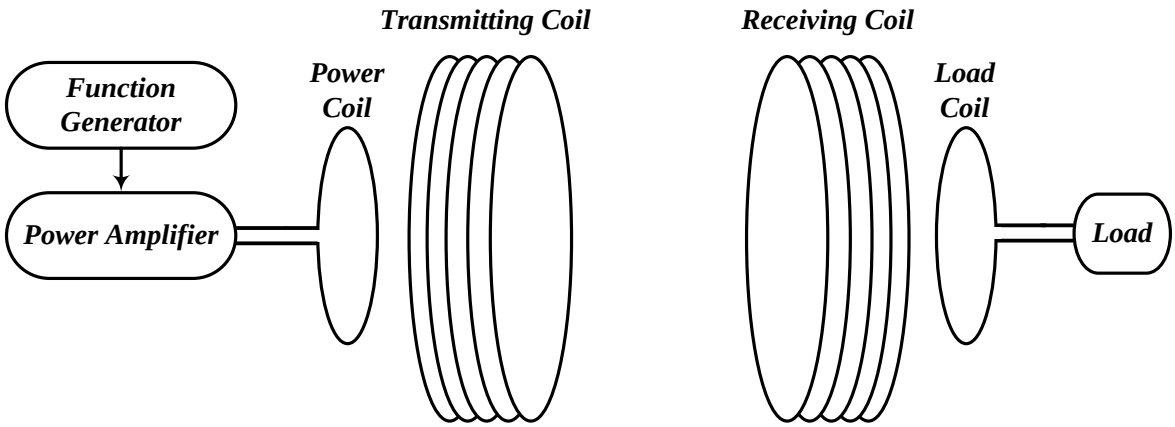

Figure 2-3: Model of magnetic resonance based WPT system.

Figure 2-4 shows the circuit representation of the four-coil system as modeled above. The schematic is composed of four resonant circuits corresponding to the four coils. These coils are connected together with a magnetic field, characterized by coupling coefficients k_{12}, k_{23}, and k_{34}. Because the strengths of cross couplings between the power coil and Rx coil, and the load coil Tx coil are very weak due to utilizing Tx and Rx resonators with multiple of coil turns, they can be neglected in the following analysis. Theoretically, the coupling coefficient has a range from 0 to 1. If all magnetic flux generated from a transmitting coil is able to reach a receiving coil, the coupling coefficient would be "1". On the contrary, the coefficient would be represented as "0" when there is no interaction between them. Actually, there are some factors identifying the coupling coefficient. It is effectively determined by the distance between the coils and their relative sizes. It is additionally determined by shapes of the coils and orientation between them. The coupling coefficient can be calculated by using a given formula

$$k_{xy} = \frac{M_{xy}}{\sqrt{L_x L_y}} \tag{2.14}$$

Where M_{xy} is mutual inductance between coil "x" and coil "y" and note that $0 \leq k_{xy} \leq 1$. Referring to the circuit schematic, an AC power source with output impedance of R_s provides energy for the system via the power coil. Normally, the AC power supply can be either a power amplifier or a vector network analyzer (VNA) which is useful to measure a transmission and reflection ratio of the system. Hence, a typical value of R_S, known as the output impedance of the power amplifier or the VNA, is 50ohm. The power coil can be modeled as an inductor L_1 with a parasitic resistor R_1. A capacitor C_1 is added to make the power coil resonate at the desirable frequency. The Tx coil is a helical coil with many turns represented as an inductor L_2 with parasitic resistance R_2. Geometry of the Tx coil determines its parasitic capacitance such as stray capacitance, which is represented as C_2.

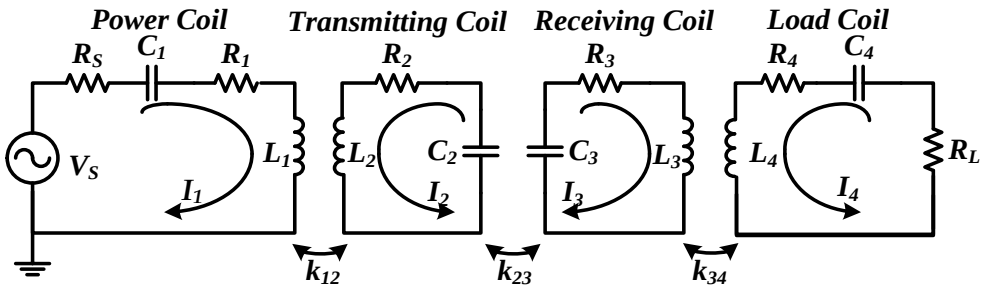

Figure 2-4: Equivalent circuit of four-coil system.

Since this kind of capacitance is difficult to be accurately predicted, for fixed size of the coil, a physical length, which impacts the self-inductance and the parasitic capacitance, has been manually adjusted in order to fit the resonant frequency as desired. In the receiver side, the Rx coil is modeled respectively by L_3, R_3 and C_3. The load coil and the connected load are also performed by L_4, R_4 and R_L. A capacitor C_4 also has the same role as C_1, so that the resonant frequency of the load coil is defined. When the frequency of sinusoidal voltage source V_S is equal to the self-resonant frequency of the resonators, their impedances are at least. In the other words, currents of the coils would be at the most and energy can be delivered mostly to the receiving coil. Otherwise, energy of the transmitting power source would be dissipated in the power coil circuit itself, resulting in the very low efficiency. In general, setting the frequency of AC supply source as same as the natural resonant frequency of the transceiver coils is one of key points to achieve a higher performance of the system.

As can be seen from figure 2-4, the Tx coil is magnetically coupled to the power coil by the coupling coefficient k_{12}. In fact, the power coil is one of the forms of impedance matching mechanism. The same situation experiences in the receiving part where the Rx coil and load coil are magnetically linked by k_{34}. The strength of interaction between the transmitting and receiving coils is characterized by the coupling coefficient k_{23}, which is decided by the distance between these coils, a relative orientation and alignment of them. In general, it is able to use other mechanisms for the impedance matching purpose in either or both sides of the system. For example, a transformer or an impedance matching network, which consists of a set of inductors and capacitors configured to connect the power source and the load to the resonators, is routinely employed. Similar to aspects mentioned above, in reality, the power and Tx coils would be implemented monolithically for the sake of convenience; hence the coupling coefficient k_{12} would be stable. For the same objective, k_{34} would also be fixed. Therefore, there only remains coefficient k_{23} which is so-called an environment variable parameter. The parameter varying with usage of conditions may include the range between the resonator coils, a relative orientation and alignment between them and a variable load on the receiving resonator.

The circuit model offers a convenient way to systematically analyze the characteristic of the system. By applying circuit theory of *Kirchhoff's Voltage Law* (KVL) to this system, with the currents in each

resonant circuit chosen as illustrated in figure 2-4, a relationship between currents through each coil and the voltage applied to the power coil can be captured as a following matrix

$$\begin{bmatrix} V_S \\ 0 \\ 0 \\ 0 \end{bmatrix} = \begin{bmatrix} Z_1 & j\omega M_{12} & 0 & 0 \\ j\omega M_{12} & Z_2 & -j\omega M_{23} & 0 \\ 0 & -j\omega M_{23} & Z_3 & j\omega M_{34} \\ 0 & 0 & j\omega M_{34} & Z_4 \end{bmatrix} \begin{bmatrix} I_1 \\ I_2 \\ I_3 \\ I_4 \end{bmatrix} \tag{2.15}$$

Where Z_1, Z_2, Z_3, and Z_4 respectively are loop impedances of the four coils. These impedances can be indicated as below

$$Z_1 = R_S + R_1 + j\left(\omega L_1 - \frac{1}{\omega C_1}\right) \tag{2.16}$$

$$Z_2 = R_2 + j\left(\omega L_2 - \frac{1}{\omega C_2}\right) \tag{2.17}$$

$$Z_3 = R_3 + j\left(\omega L_3 - \frac{1}{\omega C_3}\right) \tag{2.18}$$

$$Z_4 = R_L + R_4 + j\left(\omega L_4 - \frac{1}{\omega C_4}\right) \tag{2.19}$$

From the matrix (2.15), by using the substitution method, the current in the load coil resonant circuit is derived as given

$$i_4 = -\frac{j\omega^3 M_{12} M_{23} M_{34} V_S}{Z_1 Z_2 Z_3 Z_4 + \omega^2 M_{12}^2 Z_3 Z_4 + \omega^2 M_{23}^2 Z_1 Z_4 + \omega^2 M_{34}^2 Z_1 Z_2 + \omega^4 M_{12}^2 M_{34}^2} \tag{2.20}$$

It is clearly seen that the voltage across the load is equal to $V_L = -I_4 R_L$ and the relationship between the voltages of source and load is given as V_L/V_S.

The system model could be considered as a two port network. To analyze a figure of merit of this kind of system, scattering parameter is a suitable candidate. Actually, S_{21} is a vector referring to a ratio of signal exiting at an output port to a signal incident at an input port. This parameter is really important because a power gain, the critical factor determining of power transfer efficiency, is given by $|S_{21}|^2$, the squared magnitude of S_{21}. The parameter of S_{21} is calculated by [14]

Thus, combining with mutual inductance equation, the S_{21} parameter is given as

$$S_{21} = \frac{j2\omega^3 k_{12} k_{23} k_{34} L_2 L_3 \sqrt{L_1 L_4 R_S R_L}}{Z_1 Z_2 Z_3 Z_4 + k_{12}^2 L_1 L_2 Z_3 Z_4 \omega^2 + k_{23}^2 L_2 L_3 Z_1 Z_4 \omega^2 + k_{34}^2 L_3 L_4 Z_1 Z_2 \omega^2 + k_{12}^2 k_{34}^2 L_1 L_2 L_3 L_4 \omega^4} \tag{2.21}$$

And using the matrix (2.15) with quality factor equation, substituted each equations. The current of the power coil circuit could be derived as follow

$$i_1 = \frac{\left(1+k_{23}^2 Q_2 Q_3 + k_{34}^2 Q_3 Q_4\right) V_S}{\left[\left(1+k_{12}^2 Q_1 Q_2\right)\left(1+k_{34}^2 Q_3 Q_4\right)+k_{23}^2 Q_2 Q_3\right] R_S} \tag{2.22}$$

Assuming input impedance equal to R_S, it is possible to get equation about coupling coefficient k_{12}

$$k_{12} = \sqrt{\frac{1}{Q_1 Q_2}\left(1+\frac{k_{23}^2 Q_2 Q_3}{1+k_{34}^2 Q_3 Q_4}\right)} \tag{2.23}$$

This result could be explained the Rx coil and load coil are fixedly attached in certain position then coupling coefficient k_{34} is not changed. Therefore, dealing with the issue of mobility and flexibility in terms of distance variations which result in change of coupling coefficient k_{23}, it is possibly to adjust the coupling coefficient k_{12} of the coils only in the transmitter side to improve the efficiency.

2.4 Input impedance about wireless power transfer system with magnetic resonance

To design the input impedance of the wireless power transfer with magnetic resonance, currents are defined. The current is shown in Figure 2-5.

The basic definition for the input impedance of the modeling is $Z_{in} = V_{in} / I_{in}$. Two mutually inductive elements shown in Figure 2-6 have voltages defined in equations (2.24) and (2.25) as follow

$$v_1 = -M\frac{\delta i_2}{\delta t} \tag{2.24}$$

$$v_2 = -M\frac{\delta i_2}{\delta t} \tag{2.25}$$

But above equations are time-dependent values. Considering steady state, equation (2.24) and (2.25) become (2.26) and (2.27).

$$V_1 = -j\omega M I_2 \tag{2.26}$$

$$V_2 = -j\omega M I_1 \tag{2.27}$$

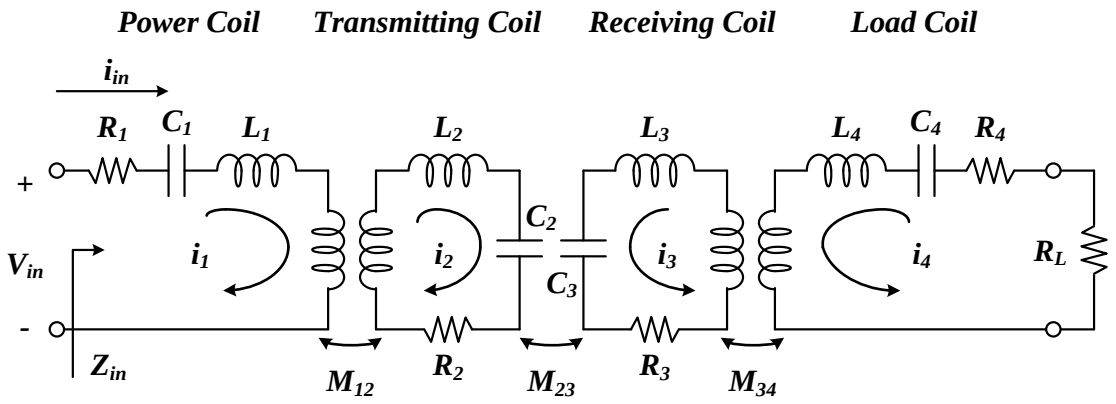

Figure 2-5: Lumped components circuit modeling with currents.

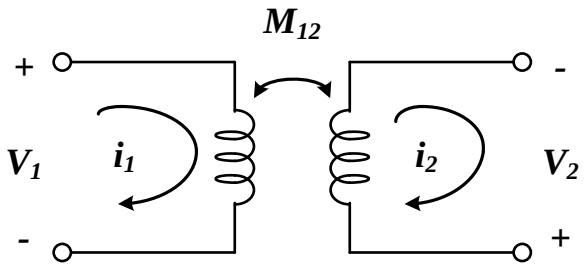

Figure 2-6: Two mutual components with relevant currents and voltages.

With these definitions and neglect receiver term, *Kirchhoff's Voltage Law* could be produced

$$V_{in} = i_1 R_1 + j\omega L_1 i_1 + \frac{i_1}{j\omega C_1} - j\omega M_{12} i_2 \tag{2.28}$$

$$j\omega M_{12} i_1 = i_2 R_2 + j\omega L_2 i_2 + \frac{i_2}{j\omega C_2} \tag{2.29}$$

From (2.29), i_2 is solved as a function of i_1.

$$i_2 = \frac{j\omega M_{12} i_1}{R_2 + j\omega L_2 - \dfrac{j}{\omega C_2}} \tag{2.30}$$

Then, (2.30) is inserted into (2.28).

$$V_{in} = i_1 R_1 + j\omega L_1 i_1 - \frac{j}{\omega C_1} i_1 + \frac{\left(\omega M_{12}\right)^2}{R_2 + j\omega L_2 - \dfrac{j}{\omega C_2}} i_1 \tag{2.31}$$

From the circuit model of the Figure 2.5, it is possible to define that $I_{in} = i_1$. This defines the input impedance as follow

$$Z_{in} = \frac{V_{in}}{I_{in}} = R_1 + j\left(\omega L_1 - \frac{1}{\omega C_1}\right) + \frac{\left(\omega M_{12}\right)^2}{R_2 + j\left(\omega L_2 - \frac{1}{\omega C_2}\right)} \tag{2.32}$$

2.5 Output impedance about wireless power transfer system with magnetic resonance

The output impedance of wireless power transfer system, Z_{out}, is related with input impedance. The method of derivation is similar to input impedance derivation. In this system, the output impedance has duality.

$$Z_{out} = R_4 + j\left(\omega L_4 - \frac{1}{\omega C_4}\right) + \frac{\left(\omega M_{34}\right)^2}{R_3 + j\left(\omega L_3 - \frac{1}{\omega C_1}\right)} \tag{2.33}$$

Chapter III

Technical Approaches of Wireless Power Transfer System for Efficiency Enhancement

This chapter introduces technical approaches such as impedance transfer technique, power point of view for calculating transfer efficiency. Finally, the design of fully system to implement wireless power transfer system needs radio frequency directional coupler. That's why the end of this chapter is stated.

3.1 Efficiency determination of wireless power transfer system by using scattering parameters

The wireless power transfer system could be analyzed by using scattering matrix's parameters with assumption of two-port network, which is shown in figure 3-1. As described in [15], complex networks could be characterized by various equivalent circuit parameters, such as impedance and admittance matrices, scattering matrix, and transmission matrix. Especially, the wireless power transfer system could be easily explained by two-port network.

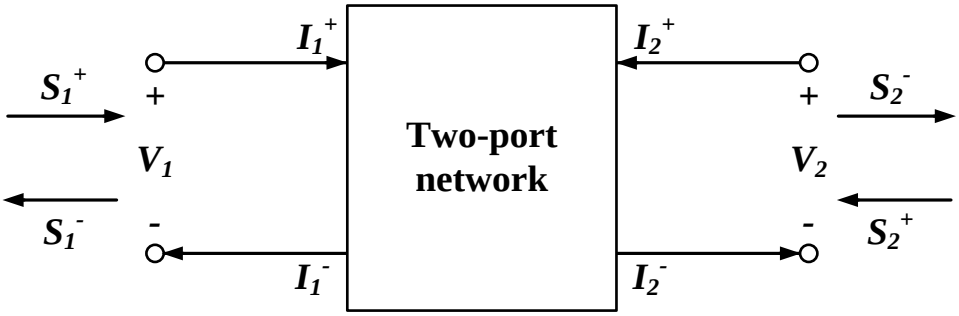

Figure 3-1: A two-port network.

Now at the two-terminal plane, the total voltage and current is given by

$$V_n = V_n^+ + V_n^- \tag{3.1}$$

$$I_n = I_n^+ - I_n^- \tag{3.2}$$

The impedance matrix [Z] of the two-port network then relates these voltages and currents.

$$\begin{bmatrix} V_1 \\ V_2 \end{bmatrix} = \begin{bmatrix} Z_{11} & Z_{12} \\ Z_{21} & Z_{22} \end{bmatrix} \begin{bmatrix} I_1 \\ I_2 \end{bmatrix} \tag{3.3}$$

From *Ohm's Law* as

$$\begin{bmatrix} I_1 \\ I_2 \end{bmatrix} = \begin{bmatrix} Y_{11} & Y_{12} \\ Y_{21} & Y_{22} \end{bmatrix} \begin{bmatrix} V_1 \\ V_2 \end{bmatrix} \tag{3.4}$$

And in practice various networks consist of a cascade connection. In this case transmission matrix is powerful to analyze the RF system. The transmission matrix is defined for a two-port network in terms of the total voltages and currents as shown

$$\begin{bmatrix} V_1 \\ I_1 \end{bmatrix} = \begin{bmatrix} A & B \\ C & D \end{bmatrix} \begin{bmatrix} V_2 \\ I_2 \end{bmatrix} \tag{3.5}$$

Where V_1 and V_2 are the input and output voltage of the network and similarly I_1 and I_2 are input and output currents with the direction shown as in a figure 3-1. Scattering matrix relates the S_1^+, S_2^+ and the S_1^-, S_2^- in figure 3-1.

$$\begin{bmatrix} V_1^- \\ V_2^- \end{bmatrix} = \begin{bmatrix} S_{11} & S_{12} \\ S_{21} & S_{22} \end{bmatrix} \begin{bmatrix} V_1^+ \\ V_2^+ \end{bmatrix} \tag{3.6}$$

Impedance, admittance, and transmission matrices are commonly used to analysis in the RF system, but the measurement of parameters is difficult. While a scattering matrix is preferred due to the vector network analyzers, which could be measured scattering parameters in the RF system.

To apply this two-port network, the efficiency of wireless power transfer between the power source and the load could be calculated as following [15].

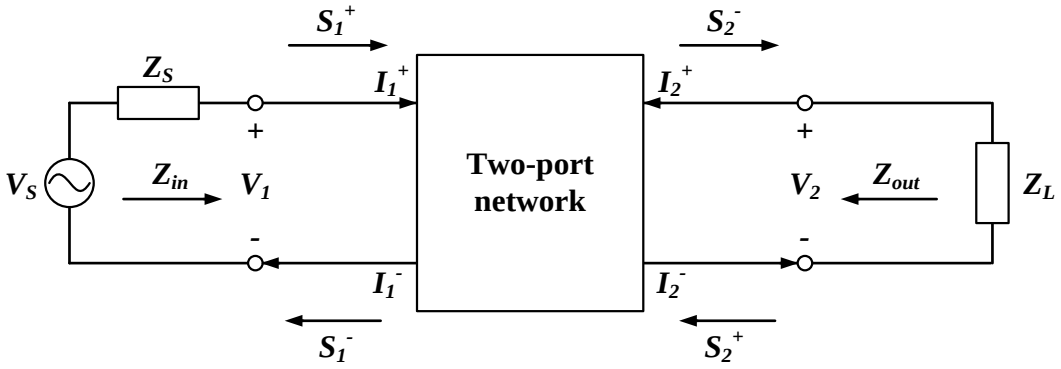

Figure 3-2: Two-port network connected to the power source and a load.

From the scattering matrix, the expression for the voltages and currents could be shown as (3.7) and (3.8).

$$V_1 = \sqrt{Z_0}\left(S_1^+ + S_1^-\right), \quad V_2 = \sqrt{Z_0}\left(S_2^+ + S_2^-\right) \tag{3.7}$$

$$I_1 = \frac{1}{\sqrt{Z_0}}\left(S_1^+ - S_1^-\right), \quad I_2 = \frac{1}{\sqrt{Z_0}}\left(S_2^+ - S_2^-\right) \tag{3.8}$$

Where Z_0 is the characteristic impedance typically selected to be 50ohm. From figure 3-2, equation (3.7), and (3.8), it is possible to define scattering matrix equation as (3.9).

$$\begin{aligned} V_1 &= Z_{in} I_1 \\ V_2 &= Z_L I_2 \end{aligned} \quad \Leftrightarrow \quad \begin{aligned} S_1^- &= \Gamma_{in} S_1^+ \\ S_2^- &= \Gamma_L S_2^+ \end{aligned} \tag{3.9}$$

Where Z_{in} is the input impedance of the two-port network and Γ_{in}, Γ_L are the reflection coefficients given by (3.10) and (3.11).

$$\Gamma_{in} = \frac{Z_{in} - Z_0}{Z_{in} + Z_0} \tag{3.10}$$

$$\Gamma_L = \frac{Z_L - Z_0}{Z_L + Z_0} \tag{3.11}$$

From (3.7) to (3.11), it is possible to calculate reflection coefficients by using scattering parameters.

$$\Gamma_{in} = S_{11} + \frac{S_{12} S_{21} \Gamma_L}{1 - S_{22} \Gamma_L} \tag{3.12}$$

To follow the method in [15], if the positions of the power source and the load are reversed, two reflection coefficients could be derived as (3.13) and (3.14).

$$\Gamma_{out} = \frac{Z_{out} - Z_0}{Z_{out} + Z_0} \tag{3.13}$$

$$\Gamma_S = \frac{Z_S - Z_0}{Z_S + Z_0} \tag{3.14}$$

Where Z_{out} is the output impedance in the two-port network, and the reflection coefficients in (3.13) and (3.14) also could be described as (3.15).

$$\Gamma_{out} = S_{22} + \frac{S_{12}S_{21}\Gamma_S}{1 - S_{11}\Gamma_S} \tag{3.15}$$

The efficiency of the wireless power transfer can be deduced through the power delivered to the two-port network, P_{in} and the power delivered to the load, P_L. For the two-port system, the input and output delivered power could be described as (3.16) and (3.17).

$$P_{in} = \frac{1}{2}\left|V_S\right|^2 \frac{R_{in}}{\left|Z_{in} + Z_S\right|^2} \tag{3.16}$$

$$P_L = \frac{1}{2}\left|V_S\right|^2 \frac{R_L \left|Z_{21}\right|^2}{\left|\left(Z_{11} + Z_S\right)\left(Z_{out} + Z_L\right)\right|^2} \tag{3.17}$$

By using equations (3.16) and (3.17), it is possible to assume essential conditions of maximum power delivery from power source to load. The conditions are given by (3.18) and (3.19).

$$Z_{in} = Z_S^* \tag{3.18}$$

$$Z_L = Z_{out}^* \tag{3.19}$$

This condition is known as conjugate matching, and results in maximum power transfer efficiency to the load, for fixed power source impedance. And the efficiency of wireless power transfer could be derived as (3.20).

$$\eta = \frac{\left(1 - \left|\Gamma_S\right|^2\right)\left|S_{21}\right|^2\left(1 - \left|\Gamma_L\right|^2\right)}{\left|\left(1 - S_{11}\Gamma_S\right)\left(1 - S_{22}\Gamma_L\right) - S_{12}S_{21}\Gamma_S\Gamma_L\right|^2} \tag{3.20}$$

From the conjugate matching condition, if the load and source impedance are matched to the characteristic impedance, reflection coefficients could be derived as (3.21).

$$\Gamma_S = \Gamma_L = 0 \quad \text{and} \quad \Gamma_{in} = S_{11}, \quad \Gamma_{out} = S_{22} \tag{3.21}$$

And substituting (3.21) to (3.20) the efficiency equation could be simplified as (3.22).

$$\eta = \left|S_{21}\right|^2 \tag{3.22}$$

3.2 Definition of parameters for improving wireless power transfer efficiency

Before the additional circuit design, it is necessary to know the various parameters such as voltage standing wave ratio, insertion loss, reflection loss, reflection coefficient, and delivered power.

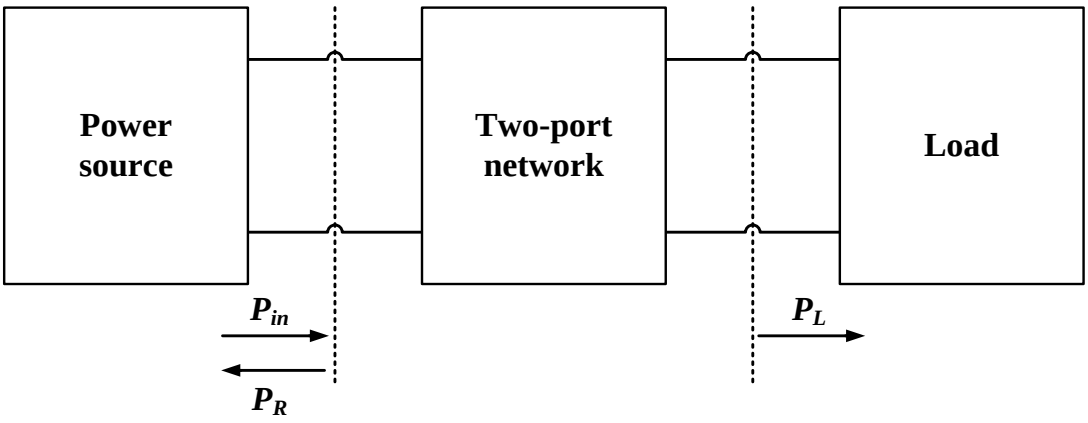

Figure 3-3: Network of general radio frequency system.

In figure 3-3, parameters could be described as input power from power source P_{in}, reflected power from two-port network to power source P_R, and delivered power to load P_L. where insertion loss (IL) could be defined as equation (3.23).

$$IL = -10\log\left(\frac{P_L}{P_{in}}\right) \tag{3.23}$$

If IL equal to 3dB, it is meaningful to deliver power from source to load. And return loss (RL) is following (3.24).

$$\begin{aligned} RL &= -10\log\left(\frac{P_R}{P_{in}}\right) \\ &= -10\log\left(\frac{VSWR-1}{VSWR+1}\right) \\ &= -10\log\left|\Gamma_{in}\right|^2 \end{aligned} \tag{3.24}$$

To summarize,

Return Loss (dB)	Reflection Coefficient	VSWR	Insertion Loss (dB)	Delivered Power (%)
0	1.0000	Infinite	infinite	0
0.5	0.09441	34.75	9.64	10.87
1	0.8913	17.39	6.87	20.6
2	0.7943	8.72	4.33	36.9
3	0.7079	5.85	3.02	49.9
4	0.6310	4.42	2.20	60.2
6	0.5012	3.01	1.26	74.9
8	0.3981	2.32	0.75	84.2
10	0.3162	1.93	0.46	90.0
12	0.2512	1.67	0.28	93.7
15	0.1778	1.43	0.14	96.8
20	0.1000	1.22	0.04	99.0
25	0.0560	1.12	0.01	99.7
30	0.0316	1.07	< 0.01	99.9

Table 3-1: Insertion loss, return loss, and related parameters.

3.3 Impedance transfer technology for improving wireless power transfer efficiency

The purpose of the impedance transfer technology in typical radio frequency system like the configuration shown in figure 3-4, which shows an impedance matching network placed between the load and the characteristic impedance. The matching network is existed to avoid unnecessary loss of power. If this is not putted between the load impedance and the characteristic impedance, part of the input power is reflected back to the input side in case of mismatch condition.

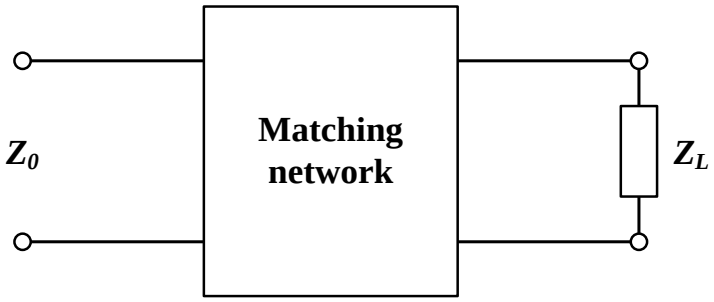

Figure 3-4: Placement of the matching network between the characteristic impedance and the load impedance.

The matching network is ideally lossless, so that no additional power is lost due to the connection of the each network, and is designed so that the impedance seen when looking from the input side into the matching network equal to the load impedance. This scheme avoids reflections back to the input side, although reflections occur between the matching network and the load impedance. Where the perfect matching is established, the maximum power is delivered to the load.

Among matching networks, L-type matching network is the most common methods for designing impedance transfer scheme. This is the simplest method to match a source to a load connected it. Using two reactive elements, any arbitrary load impedance could be matched to the characteristic impedance. There are able to design two configurations for these systems, depending on the normalized load impedance, defined as $z_L = Z_L/Z_0$, where Z_0 represents the characteristic impedance of input side. If this load impedance is inside the $1 + jx$ circle on the Smith chart, then the configuration in figure 3-5.(a) is to be used. Otherwise, the configuration shown in figure 3-5.(b) should be used. The $1 + jx$ circle is the resistance circle on the impedance Smith chart for which $r = 1$.

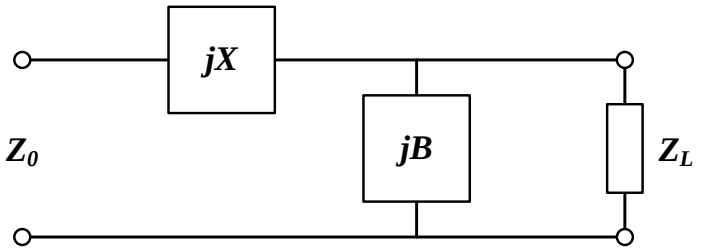

(a)

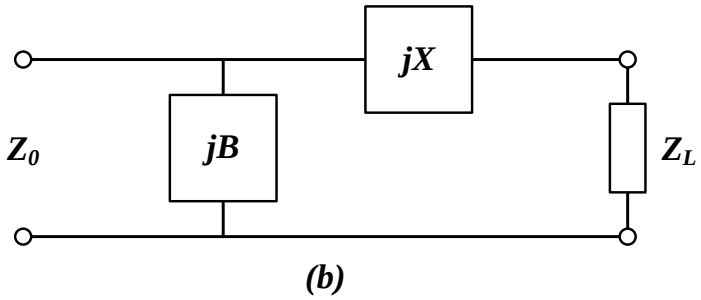

Figure 3-5: Configuration for L-type matching networks.

(a) Network for z_L inside the 1 + *jx* circle.

(b) Network for z_L outside the 1 + *jx* circle.

Regardless of which configuration is used, the reactive elements can be selected inductors or capacitors, depending on the value of the load impedance.

For example, Consider (a) case the circuit of figure 3-5.(a), and let $Z_L = R_L + jX_L$. To draw in the Smith chart is used to normalize equation that $z_L = Z_L/Z_0$ is inside the 1 + *jx* circle, which means $R_L > Z_0$. The 1 + *jx* circle is described in figure 3-6.

The impedance is looking into the matching network followed by the load impedance must be equal to Z_0, for matching condition. It is possible to describe as (3.25).

$$Z_0 = jX + \frac{1}{jB + \frac{1}{\left(R_L + jX_L\right)}} \tag{3.25}$$

From equation (3.25), it could be expressed as (3.26) and (3.27).

$$B\left(XR_L - X_L Z_0\right) = R_L - Z_0 \tag{3.26}$$

$$X\left(1 - BX_L\right) = BZ_0 R_L - X_L \tag{3.27}$$

Calculating equation (3.26) for *X* and substituting in to (3.27) gives a quadratic equation for *B.* as following

$$B = \frac{X_L \pm \sqrt{\frac{R_L}{Z_0}}\sqrt{R_L^2 + X_L^2 - Z_0 R_L}}{R_L^2 + X_L^2} \tag{3.28}$$

Since $R_L > Z_0$, the second square root term is always positive value. Then the series reactance could be found as equation (3.29).

$$X = \frac{1}{B} + \frac{X_L Z_0}{R_L} - \frac{Z_0}{BR_L} \tag{3.29}$$

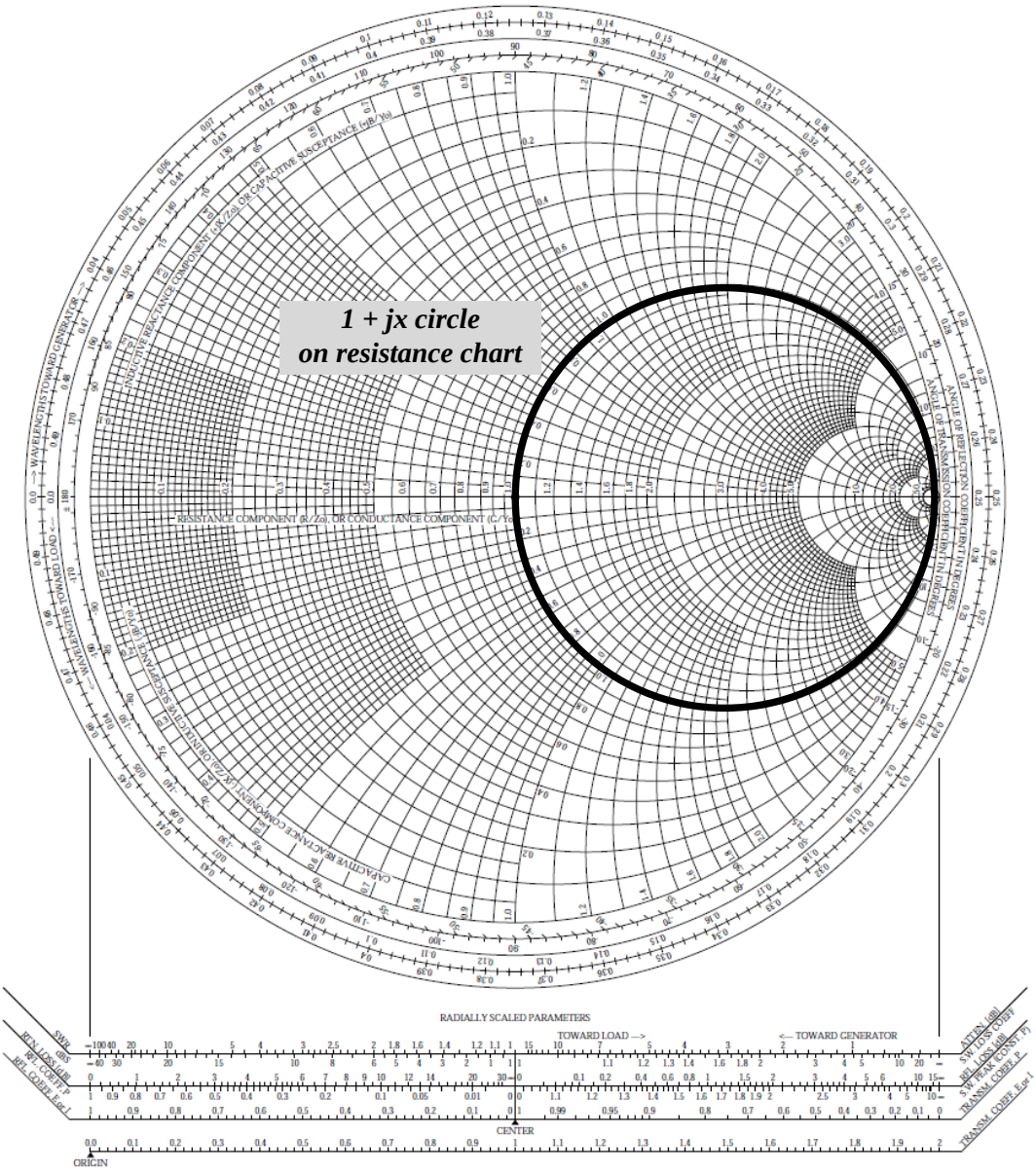

Figure 3-6: Smith chart for the L-type matching network.

Otherwise in figure 3-5.(b) case, it is possible to analyze 1 + *jx* circle using on the admittance chart, which is implies that $R_L < Z_0$. Therefore, X and B give

$$X = \pm\sqrt{R_L\left(Z_0 - R_L\right)} - X_L \tag{3.30}$$

$$B = \pm \frac{\sqrt{\left(Z_0 - R_L\right)/R_L}}{Z_0} \tag{3.31}$$

3.4 Analysis of radio frequency directional coupler based on transformer

The analysis that describes the performance of transformer based directional coupler is derived. The best theoretical performance available from a directional coupler, using ideal transformer, is a function of the turn ratio, and the terminating impedances.

At the Very High Frequency (VHF) and Ultra High Frequency (UHF), wires gauge and core material can be chosen to closely approximate the response based on the solution of these analysis.

A directional coupler separates signals based on the direction of signal propagation. These devices are used to unequally split the signal flowing in the mainline and to fully pass the signal flowing in the opposite direction.

In an ideal situation some portion of the signal flowing into port A will appear at port C. Likewise any signal flowing into port C will be coupled fully to port A. However ports B and C are isolated in that any signal flowing into port B will not appear at port C but will feed through to port A. The generic radio frequency directional coupler symbol, shown in figure 3-7.(a), is realized by two transformers connected as shown in figure 3-7.(b).

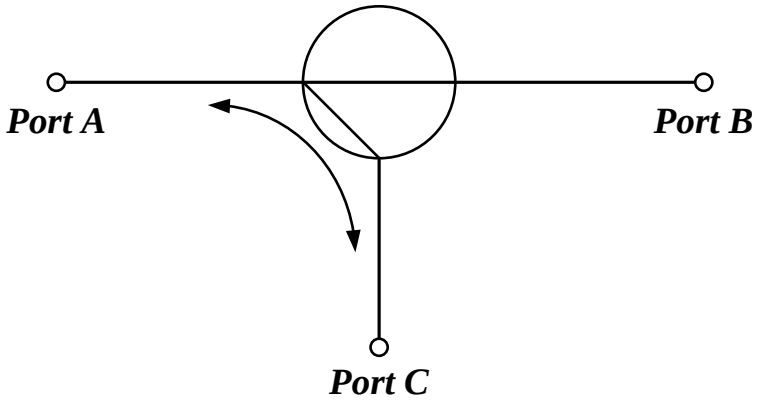

(a)

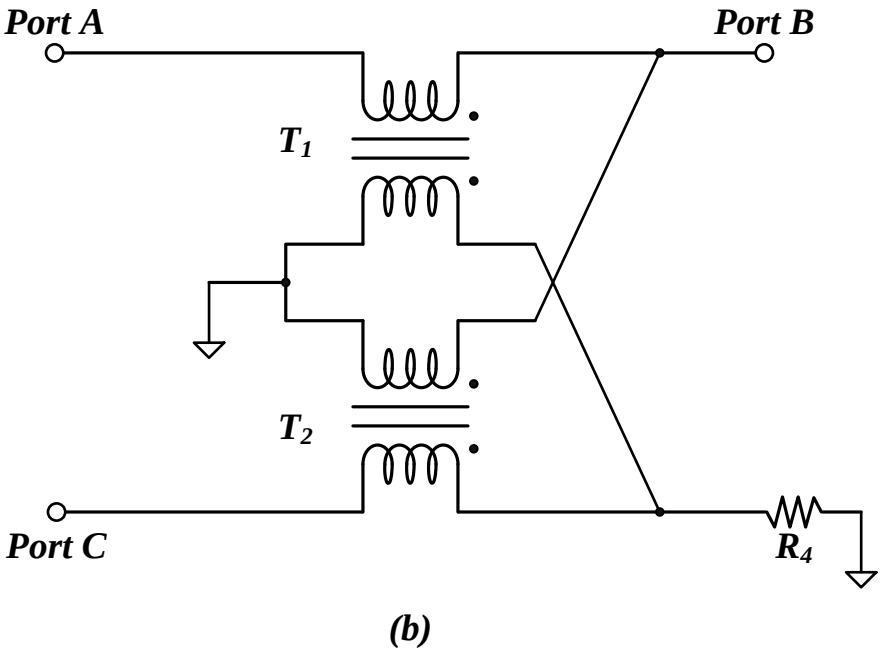

Figure 3-7: Configurations of RF directional coupler.

(a) RF directional coupler symbolic.

(b) RF directional coupler equivalent circuit.

This type has impedance, in that they become 50ohm or 75ohm, directional coupler simply by matching all ports to either 50ohm, or 75ohm, respectively.

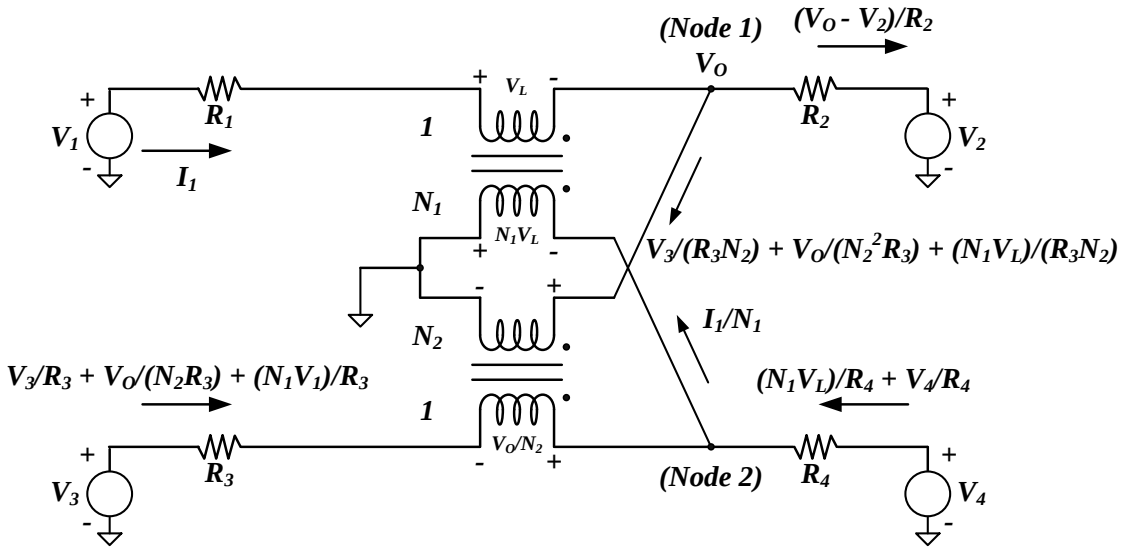

Figure 3-8: Nodal voltages and currents in a RF directional coupler.

Figure 3-8 is a generic model for analysis. In the forward mode of operation, V_1 is applied input

voltage with V_2, V_3, and V_4 replaced by shorts. V_O then becomes the output voltage. A portion of the output voltage, V_O, is coupled to R_3, and ideally no voltage appears across R_4.In the reverse mode of operation, V_2 is the applied input voltage with V_1, V_3, and V_4 replaced by shorts. The output voltage then becomes the voltage across R_1. A portion of the output voltage (voltage across R_1) is coupled to R_4, and ideally no voltage appears across R_3.

The turn ratio of T_1 is 1:N_1 where N_1 is the secondary of the transformer T_1. Similarly, the turn ratio of T_2 is 1:N_2 where N_2 is the secondary of the transformer T_2. The location of the dots beside the transformers denotes that the voltage across the primary is in phase with the voltage across the secondary. Voltage sources are shown at all four ports because, by shorting each of the three voltages sources to ground, the input impedance of the port with the non-zero voltage source can be found from the nodal equations. The equations shown in figure 3-8 can be written down by inspection using *Ohm's Law* and *Kirchhoff's Voltage* and *Current Law*.

i. T_1 is defined to be the current through R_1.

ii. The voltage across the primary of T_1 is defined to be V_L.

iii. The voltage *Node 1* is defined to be V_O.

iv. The current flowing through R_2 is therefore the voltage across R_2, divided by R_2, or $(V_O - V_2)/R_2$.

v. The voltage across the secondary of T_1 is N_1 times the voltage across the primary of T_1, or N_1V_L.

vi. If the current through the primary of T_1 is I_1, then the current through the secondary of T_1 has to be I_1/N_1.

vii. The voltage across the secondary of T_2 has already been denoted as V_O.

viii. Therefore the voltage across the primary of T_2 has to be V_O/N_2.

ix. The current through R_3 has to be the sum of the voltage across R_3 divided by R_3. These three voltages are V_3, V_O/N_2, and N_1V_L and they add since they are all in phase. The current through R_3 becomes $V_3/R_3 + V_O/(N_2R_3) + (N_1V_L)/R_3$.

x. The current through the secondary of T_2 has to be equal to the current through R_3 divided by N_2, or $V_3/(R_3N_2) + V_O/(N_2^2R_3) + (N_1V_L)/(R_3N_2)$.

xi. The current through R_3 is equal to the voltage across of R_3 are N_1V_L and V_3, respectively. They add since they are in phase. Therefore the current through R_4 is $(N_1V_L)/R_4 + V_4/R_4$.

The current flowing into *Node 1* has to be equal to the currents flowing out of *Node 1*, therefore

$$I_1 = \frac{V_3}{R_3 N_2} + \frac{V_O}{N_2^2 R_3} + \frac{N_1 V_L}{R_3 N_2} + \frac{V_O - V_2}{R_3} \tag{3.32}$$

Also the currents flowing into *Node 2* have to be equal to the current flowing out of *Node 2*, or

$$\frac{I_1}{N_1} = \frac{V_3}{R_3} + \frac{V_O}{N_2 R_3} + \frac{N_1 V_L}{R_3} + \frac{N_1 V_L}{R_4} + \frac{V_4}{R_4} \tag{3.33}$$

It is necessary to eliminate the variable, V_L, using the equation.

$$V_L = \left(V_1 - I_1 R_1 - V_O\right) \tag{3.34}$$

Substituting equation (3.34) into (3.32) and (3.33), and rearranging each parameter, the final nodal equations become

$$\frac{V_3}{R_3} + \frac{N_1 V_1}{R_3} + \frac{N_1 V_1}{R_4} + \frac{V_4}{R_4} + V_O\left(\frac{1}{N_2 R_3} - \frac{N_1}{R_3} - \frac{N_1}{R_4}\right) = I_1\left(\frac{1}{N_1} + \frac{N_1 R_1}{R_3} + \frac{N_1 R_1}{R_4}\right) \tag{3.35}$$

And

$$\frac{V_3}{R_3 N_2} + \frac{N_1 V_1}{R_3 N_2} - \frac{V_2}{R_2} + V_O\left(\frac{1}{N_2^2 R_3} - \frac{N_1}{R_3 N_2} + \frac{1}{R_2}\right) = I_1\left(1 + \frac{N_1 R_1}{R_3 N_2}\right) \tag{3.36}$$

Equations (3.35) and (3.36) are easily solved for V_O and I_1 since V_1, V_2, V_3, and V_4 are known and only one is non-zero for a given analysis. From inspection of figure 3-8, the input impedances at each port are given by

$$\begin{aligned}
&\text{For } V_1 \neq 0, \quad R_{in1} = \frac{V_L + V_O}{I_1} \\
&\text{For } V_2 \neq 0, \quad R_{in2} = \frac{-V_O}{\dfrac{V_O - V_2}{R_2}} \\
&\text{For } V_3 \neq 0, \quad R_{in3} = \frac{V_3}{\dfrac{V_3}{R_3} + \dfrac{V_O}{N_2 R_3} + \dfrac{N_1 V_L}{R_3}} - R_3 \\
&\text{For } V_4 \neq 0, \quad R_{in4} = \frac{N_1 V_L}{\dfrac{N_1 V_L}{R_4} + \dfrac{V_4}{R_4}}
\end{aligned} \tag{3.37}$$

The return loss, R_L, at port x (for x = 1, 2, 3, or 4) is given by

$$R_{Lx} = -20\log\left(\left|\frac{R_x - R_{inx}}{R_x + R_{inx}}\right|\right) \tag{3.38}$$

In the forward direction (V_1 not equal to zero), from inspection of figure 3-8 the loss at the various ports is described as

$$\text{Forward insertion loss } = -20\log\left(\frac{V_O}{\frac{R_2}{R_1 + R_2}}\right) \tag{3.39}$$

$$\text{Forward coupled port loss } = -20\log\left(\frac{\frac{V_O}{N_2} + N_1 V_L}{\frac{R_2}{R_1 + R_2}}\right) \tag{3.40}$$

$$\text{Forward isolated port loss } = -20\log\left(\frac{N_1 V_L}{\frac{R_2}{R_1 + R_2}}\right) \tag{3.41}$$

In the reverse direction (V_2 not equal to zero), the loss at the various ports is described as

$$\text{Reverse insertion loss } = -20\log\left(\frac{I_1 R_1}{\frac{R_1}{R_1 + R_2}}\right) \tag{3.42}$$

$$\text{Reverse coupled port loss } = -20\log\left(\frac{N_1 V_L}{\frac{R_1}{R_1 + R_2}}\right) \tag{3.43}$$

$$\text{Reverse isolated port loss } = -20\log\left(\frac{\frac{V_O}{N_2} + N_1 V_L}{\frac{R_1}{R_1 + R_2}}\right) \tag{3.44}$$

Table 3-2 summarized a portion of the design data that is available from the computer aided

calculation based on the preceding equations. The return loss values in Table X are valid for any arbitrary characteristic impedance, Z_O, therefore Table 3-2 can be used to design both 50ohm and 75ohm directional coupler. In the results, the frequency range of directional coupler based on toroidal can span two decades of frequency and commonly covers the frequency of 5MHz to 1GHz.

N1	N2	Insertion Loss (dB)	Coupled Port Loss (dB)	Input Return Loss (dB)	Output Return Loss (dB)	Coupled Port Return Loss (dB)
1.0	1.0	7.96 dB	1.94 dB	14.0 dB	14.0 dB	14.0 dB
1.5	1.5	2.60 dB	3.94 dB	15.7 dB	15.7 dB	15.7 dB
2.0	2.0	1.29 dB	6.15 dB	19.4 dB	19.4 dB	19.4 dB
2.5	2.5	0.78 dB	8.01 dB	22.7 dB	22.7 dB	22.7 dB
2.5	3.0	0.65 dB	8.76 dB	26.1 dB	22.6 dB	22.6 dB
3.0	2.5	0.65 dB	8.76 dB	22.6 dB	26.1 dB	26.1 dB
3.0	3.0	0.52 dB	9.57 dB	25.6 dB	25.6 dB	25.6 dB
3.0	3.5	0.45 dB	10.2 dB	28.4 dB	25.6 dB	25.6 dB
3.5	3.0	0.44 dB	10.2 dB	25.6 dB	28.4 dB	28.4 dB
3.5	3.5	0.38 dB	10.9 dB	28.2 dB	28.2 dB	28.2 dB
3.5	4.0	0.33 dB	11.5 dB	30.6 dB	28.2 dB	28.2 dB
4.0	3.5	0.33 dB	11.5 dB	28.2 dB	30.6 dB	30.6 dB
4.0	4.0	0.28 dB	12.1 dB	30.4 dB	30.4 dB	30.4 dB
4.0	5.0	0.23 dB	13.0 dB	34.6 dB	30.5 dB	30.5 dB
5.0	4.0	0.23 dB	13.0 dB	30.5 dB	34.6 dB	34.6 dB
5.0	5.0	0.18 dB	14.0 dB	34.2 dB	34.2 dB	34.2 dB
5.0	6.0	0.15 dB	14.7 dB	37.5 dB	34.2 dB	34.2 dB
6.0	5.0	0.15 dB	14.7 dB	34.2 dB	37.5 dB	37.5 dB
6.0	6.0	0.12 dB	15.6 dB	37.3 dB	37.3 dB	37.3 dB
6.0	7.0	0.11 dB	16.2 dB	40.1 dB	37.3 dB	37.3 dB
7.0	6.0	0.11 dB	16.2 dB	37.3 dB	40.1 dB	40.1 dB
7.0	7.0	0.09 dB	16.9 dB	39.9 dB	39.9 dB	39.9 dB

Table 3-2: Directional coupler loss as function of turns ratio

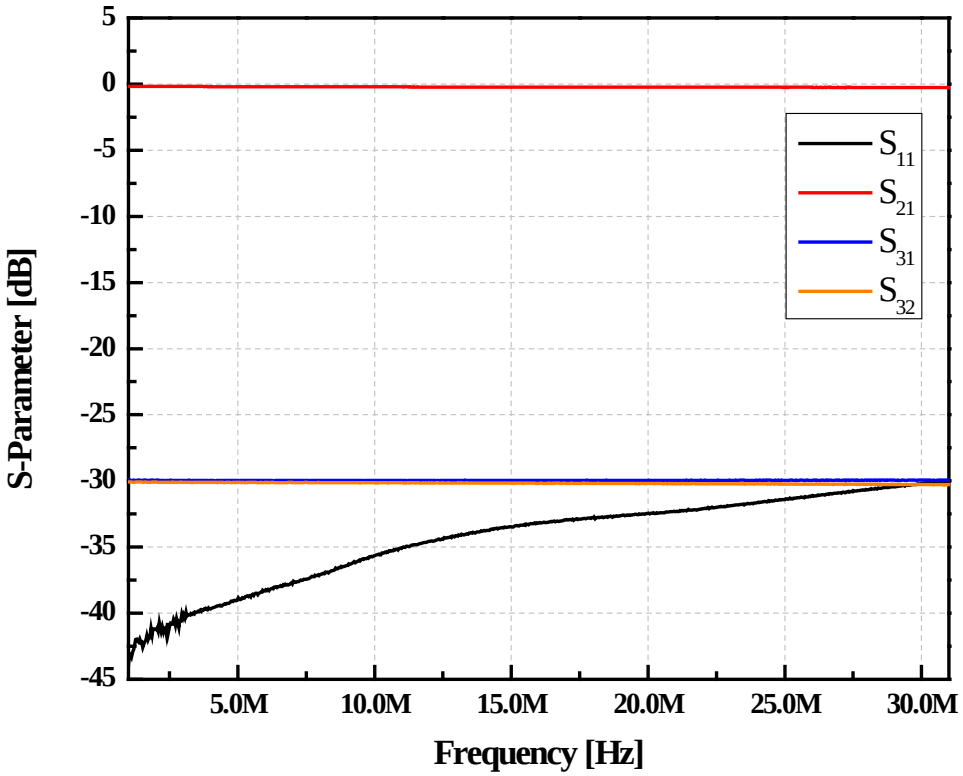

Figure 3-9: Measured scattering parameters about direction coupler.

Chapter IV

Efficiency Improvement for Wireless Power Transfer System with Magnetic Resonance

This chapter explains and describes technologies to improve efficiency of magnetic resonance based wireless power transfer system with several kinds of condition.

4.1 Efficiency improvement for magnetic resonance based wireless power transfer with axial-misalignment

4.1.1 Introduction

In 2007, [8] proposed a novel way to transmit power wirelessly using magnetic resonance, in which the optimal efficiency results were shown when two resonant devices were perfectly aligned. However, in order to build up a practical wireless power transfer system, the axial-misalignment case needs to be considered as well.

In this chapter, an adaptive method to improve the system performance in axial-misalignment condition is described. Experimental results are demonstrated to verify the effectiveness of the proposed method.

4.1.2 System analysis

In the system shown in figure 4-1, large coils that are modeled by L_1 and L_2 are connected together via a magnetic field, characterized by a mutual inductance M. It can be seen that in the transmitting side coupling capacitance is generated due to the source loop and helical coil. The same type of capacitance is experienced in the receiver side when helical coil and load loop form the two conductive loops. Such inductances and capacitances are able to determine the resonance frequency in each side. The coils of L_1 and L_2 form the resonators that resonate at the frequency of interest. The efficiency of wireless power transfer system can be modeled with mutual inductance and parasitic resistances and could be described as follows [16].

$$\eta = \frac{\omega^2 M^2 R_L}{R_1 \left(R_2 + R_L\right)^2 + \omega^2 M^2 \left(R_2 + R_L\right)} \tag{4.1}$$

Where ω is the resonant frequency of the system. R_1, R_2 are parasitic resistances of coil L_1 and L_2 respectively and R_L is the load resistance. A vector network analyzer (VNA) is useful to measure the transmission of reflection ratio of the wireless power transfer system, where load resistance, R_L is 50ohm.

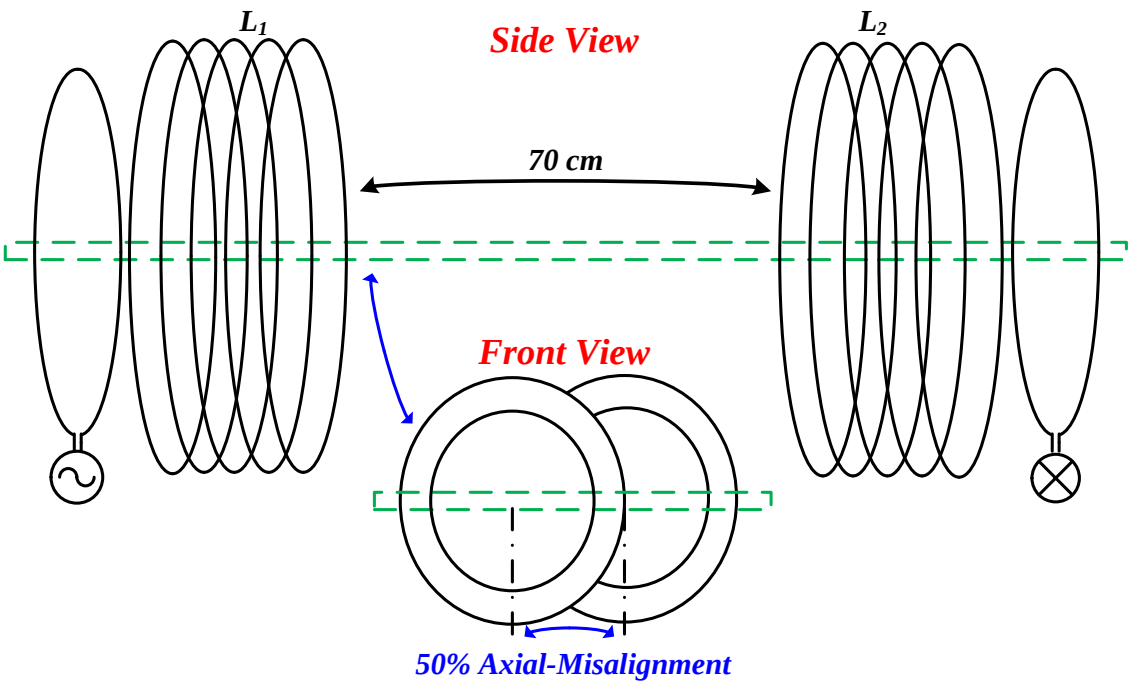

Figure 4-1: Wireless power transfer and experimental environment.

4.1.3 Proposed adaptive method

Impedance matching has commonly been used as a useful technique to improve the efficiency in wireless communication system [17]. In the case of axial-misalignment between two coils of a wireless power transfer system, the reflected power would increase causing significant decrease in wireless power transfer system performance. In this chapter, a novel method of implementing impedance matching in the transmitting side in order to reduce the reflected power enabling a wireless power transfer system with higher efficiency is proposed figure 4-1. Source impedance and load impedance are described in (4.2). In this case, the transferred power P can be presented as (4.3).

$$Z_{source} = R_{source} + jX_{source} \quad \text{and} \quad Z_{load} = R_{load} + jX_{load} \tag{4.2}$$

$$P = \frac{1}{2}|V|^2 \frac{R_{load}}{\left(R_{load} + R_{source}\right)^2 + \left(X_{load} + X_{source}\right)^2} \tag{4.3}$$

When the mismatch between source impedance and load impedance is eliminated, the transferred power in the wireless power transfer system could be described as (4.4)

$$P = \frac{1}{2}|V|^2 \frac{1}{4R_{source}} \tag{4.4}$$

The proposed technique to increase the power transfer performance is implemented with an impedance matching circuit for the case with axial-misalignment of the magnetic resonance wireless power transfer system.

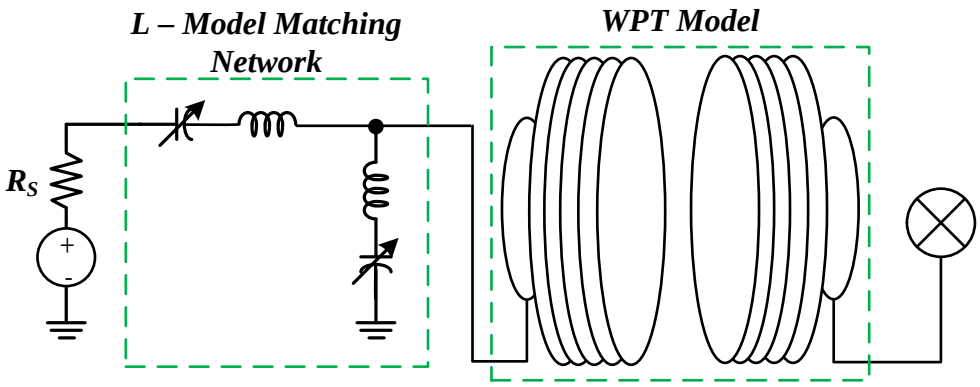

Figure 4-2: Block diagram of L-model matching network in wireless power transfer system.

4.1.4 Experimental results

The above optimization technique for wireless power transfer systems with axial-misalignment has been verified by Advance Design System (ADS), EMPro, and HFSS, in addition to experimental implementation using the model in [8]. The system consists of the source coil, transmitting helical coil (Tx coil), receiving helical coil (Rx coil) and load coil. The Tx and Rx coils, also known as the resonators, are designed to resonate at the same frequency. The transmitting side consists of a power coil with 49 cm diameter and the Tx coil that is a helical type with 60 cm diameter and 5.25 turns. The symmetric structure is duplicated on the receiving side for the load coil and Rx coil. These four coils were implemented with a 6 mm-diameter copper wire coated with gold and has a pitch of 4 cm. The measured resonant frequency of the implemented system was 10.14 MHz. As can be seen in figure 4-1., the distance between the two resonators was set at 70 cm and we intentionally introduced an axial-misalignment by 50% that is equivalent to 35 cm axial separation.

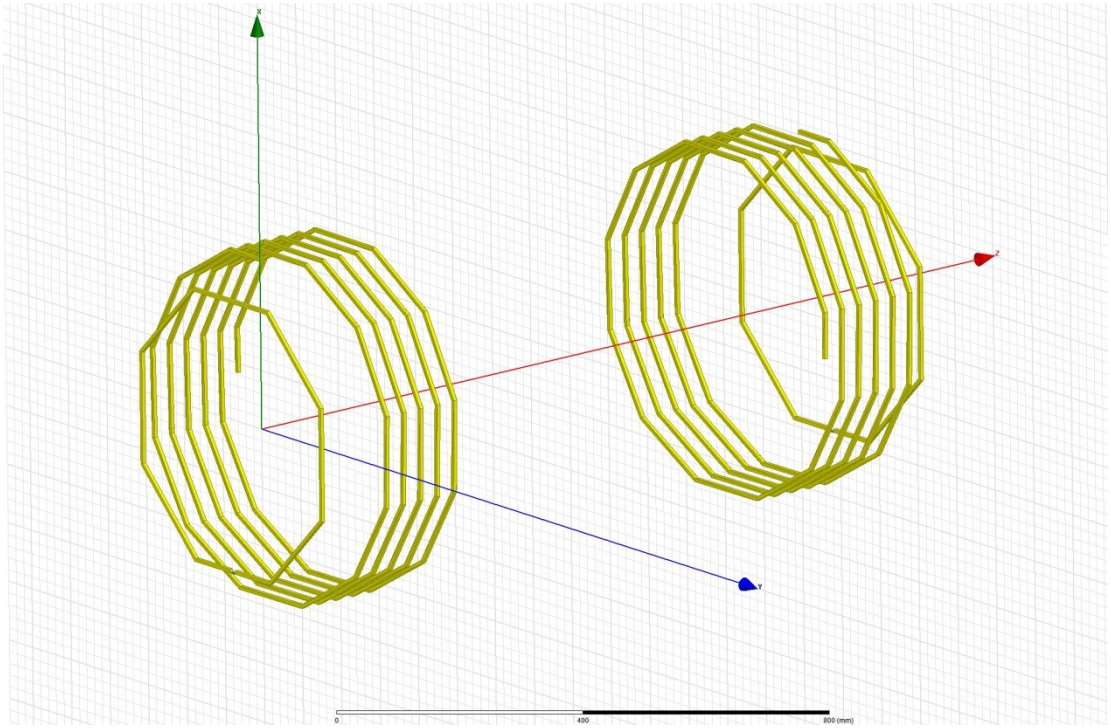

Figure 4-3: Simulated model without axial-misalignment in HFSS.

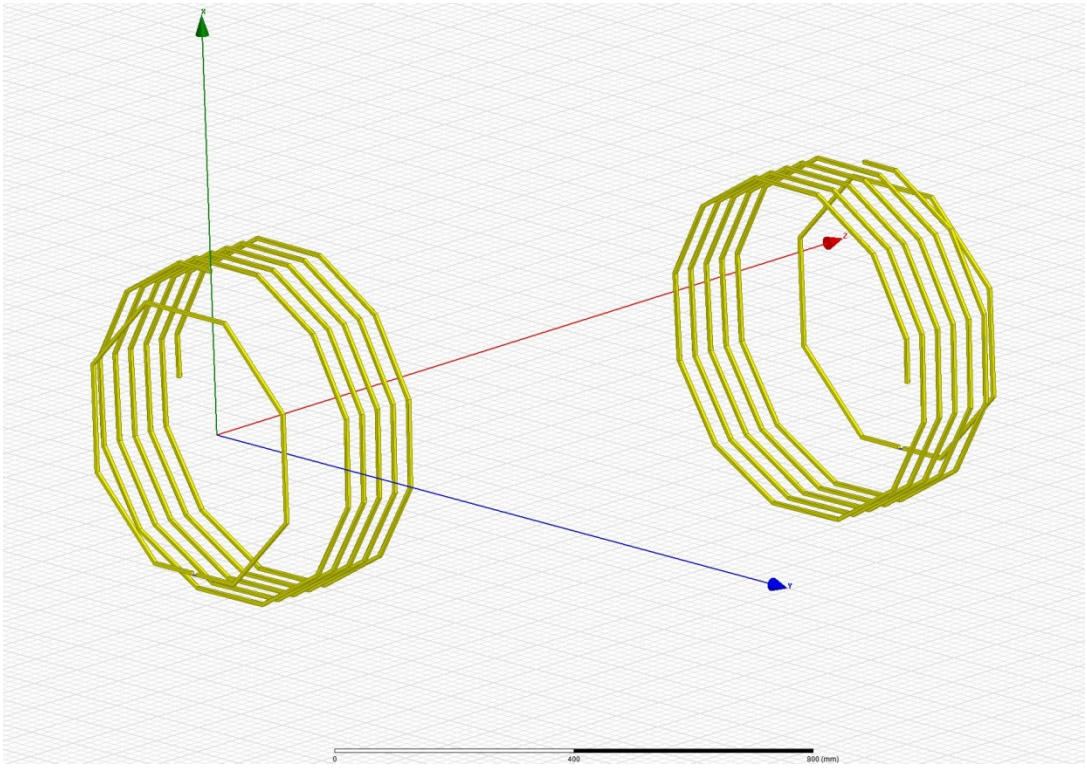

Figure 4-4: Simulated model with axial-misalignment in HFSS.

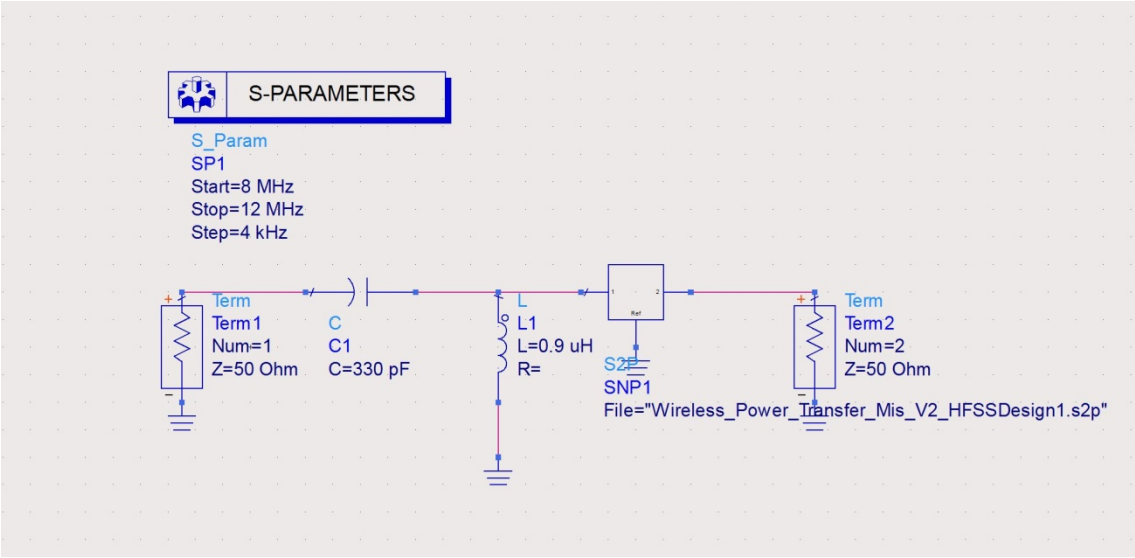

Figure 4-5: Extracted model above HFSS results in ADS and matched parameters.

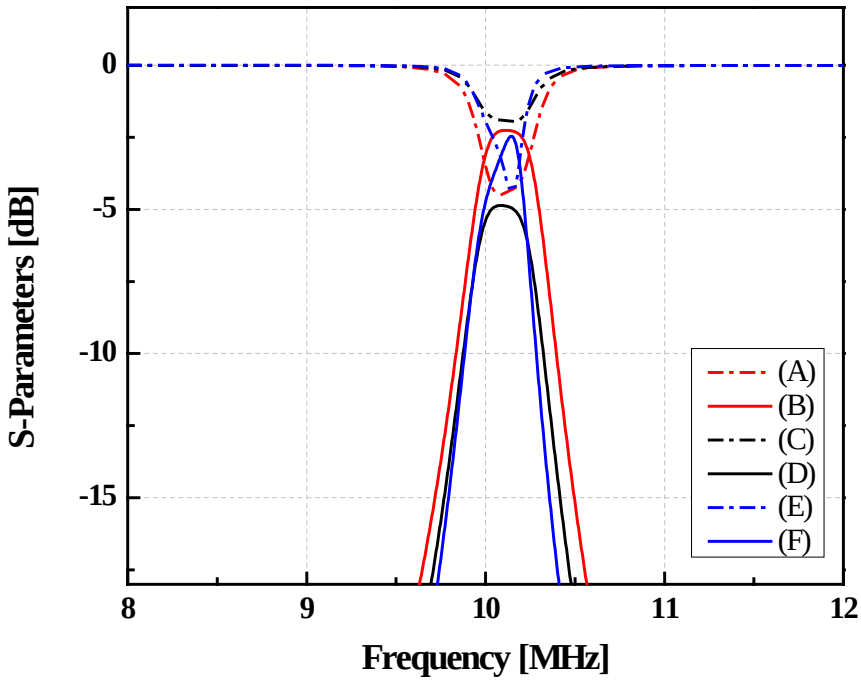

Figure 4-6: Simulated scattering parameters.

(A) S11 without axial-misalignment and matching.

(B) S21 without axial-misalignment and matching.

(C) S11 with axial-misalignment and without matching.

(D) S21 with axial-misalignment and without matching.

(E) S11 with axial-misalignment and matching.

(F) S21 with axial-misalignment and matching.

An Agilent Technologies 8751A vector network analyzer (VNA) was used for the scattering parameter measurement. Without the proposed matching circuit, the measured S_{21} is -4.1 dB. With the proposed impedance matching circuit in the wireless power transfer system, the S_{21} parameter representing the efficiency in the wireless power transfer link is increased by 1.5 dB to -2.9 dB. This measurement result corresponds to 11.4% improvement in S_{21}, or 48.4% of relative efficiency improvement compared to a wireless power transfer link without the proposed matching circuits in figure 4-8.

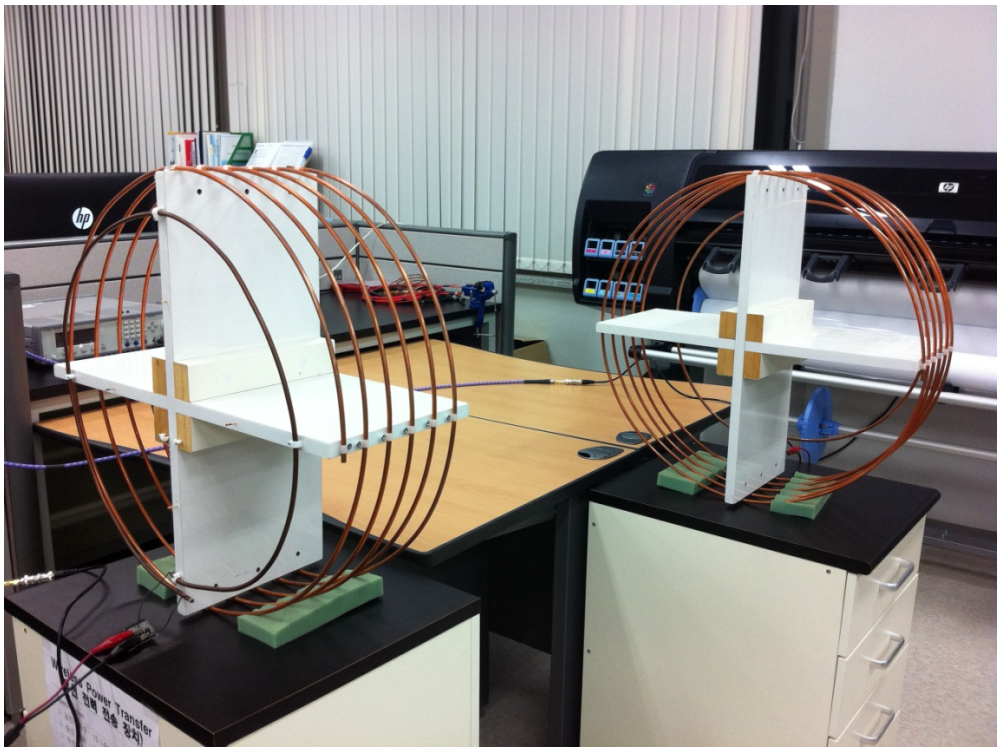

(A)

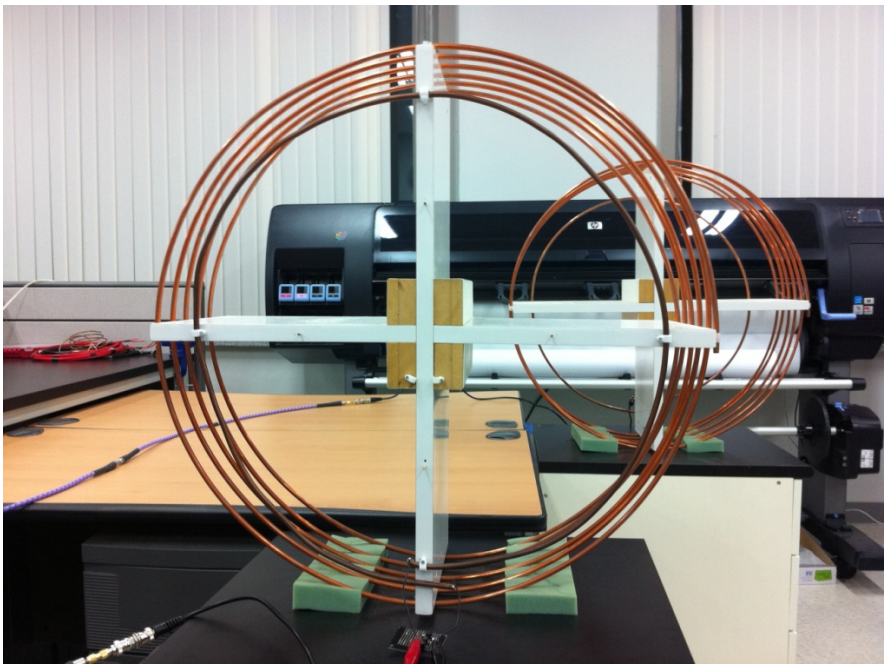

(B)

Figure 4-7: Experimental setup (A): Side view, (B): Front view

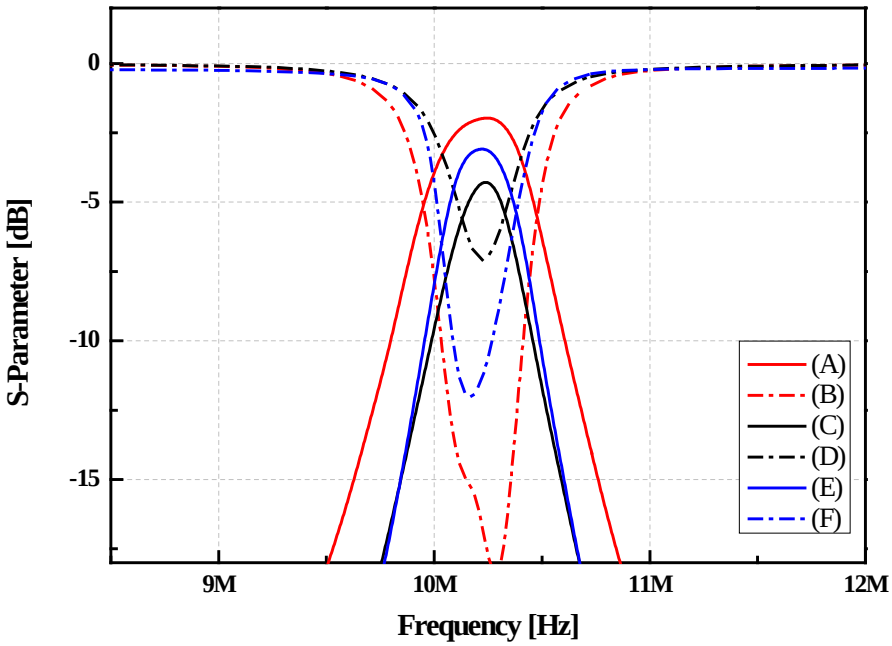

Figure 4-8: Measured scattering parameters.

(A) S21 without axial-misalignment and matching.

(B) S11 without axial-misalignment and matching.

(C) S21 with axial-misalignment and without matching.

(D) S11 with axial-misalignment and without matching.

(E) S21 with axial-misalignment and matching.

(F) S11 with axial-misalignment and matching.

4.2 Efficiency improvement for magnetic resonance based wireless power transfer with adaptive method

4.2.1 Introduction

Medium-range wireless power transfer with magnetic resonance is a growing research area that finds wide applications. It is clear that the larger sizes of transceivers, the higher efficiency of the system. However, there exists a drawback of low efficiency due to varied distance and small size receiver, in case of applications for mobile consumer electronics. The concept of using coupling between asymmetric resonators with different sizes was proposed in [18]. Nonetheless, no optimization method and theoretical analysis were reported. Since the technique in [19] seems to be impractically applied in consumer electronics, in this section, a model and an equivalent circuit of WPT system are introduced, and an adaptive method to optimize the system with respect to distance variations is presented. Simulation and experimental results are shown to clarify the analysis.

4.2.2 Theoretical analysis

A schematic of the wireless power transfer system with magnetic resonance for future portable consumer electronics devices is illustrated in figure 4-9, which consists of four one-turn loop coils, a power coil, a transmitting coil (Tx coil), a receiving coil (Rx coil) and a load coil. The Tx and Rx coils are also called resonators, which are supposed to resonate at the same frequency. As mentioned, the coils in the receiver side are needed to be scaled and supposed to be planar-sized for integration in handheld devices. Otherwise, it is quite free to determine sizes of the transmitter. D_1 is the distance between two coils in the transmitting part. D_2, which is the distance between the Tx coil and the coils in receiving side, is considered as the distance for power transfer. Figure 4-10 illustrates an equivalent

circuit representation of the model.

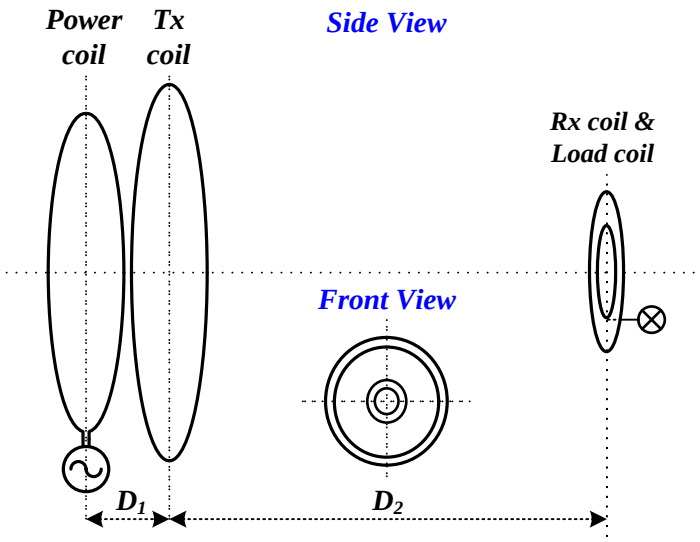

Figure 4-9: Experimental environment of WPT system with fixed receiver.

The four coils are connected together with a magnetic field, characterized M_{xy} which shows the mutual inductance between the *x*-th and the *y*-th coil. Each coil is represented by lumped components *R*, *L* and C.

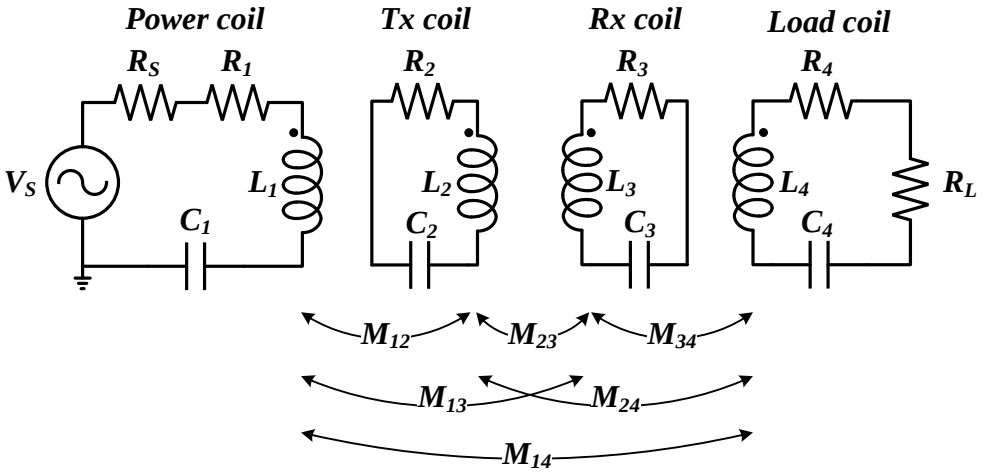

Figure 4-10: Equivalent circuit of the WPT system.

By applying the circuit theory, a relationship between currents through each coil and a voltage source V_S is obtained in the matrix below

$$\begin{bmatrix} V_S \\ 0 \\ 0 \\ 0 \end{bmatrix} = \begin{bmatrix} Z_1 & j\omega M_{12} & -j\omega M_{13} & -j\omega M_{14} \\ j\omega M_{12} & Z_2 & -j\omega M_{23} & -j\omega M_{24} \\ -j\omega M_{13} & -j\omega M_{23} & Z_3 & j\omega M_{34} \\ -j\omega M_{14} & -j\omega M_{24} & j\omega M_{34} & Z_4 \end{bmatrix} \begin{bmatrix} I_1 \\ I_2 \\ I_3 \\ I_4 \end{bmatrix} \tag{4.5}$$

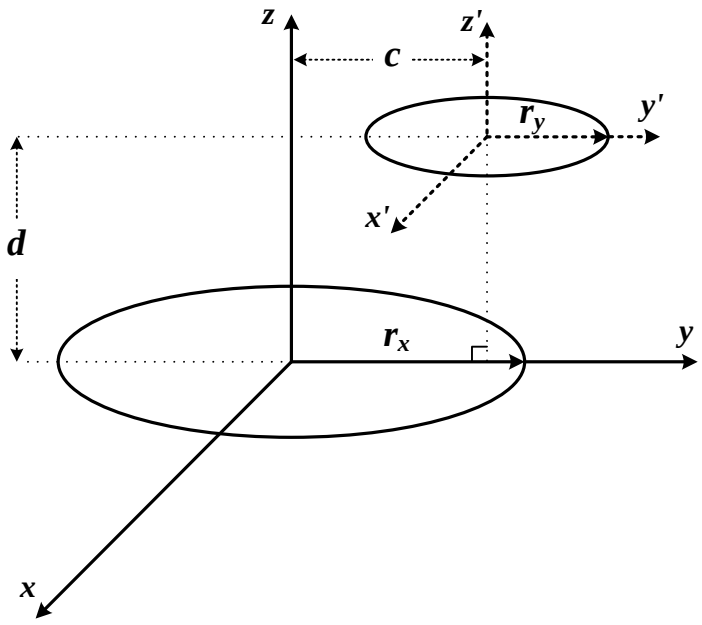

Figure 4-11: Two coils in parallel axes with variables defined for all positions.

Where Z_1, Z_2, Z_3, Z_4 are the impedance in each loop as mentioned in (2.16) to (2.19). The mutual inductance M_{xy} of two circular coils with parallel axes has been derived in [12]. Figure 4-11 shows all relevant variables for calculations. The mutual inductance M_{xy} between the two coils in figure 4-11, one with radius r_x, and the other with radius r_y, with a distance d between their axes and a distance c between plans of the coils, can be calculated as below

$$M_{xy} = \frac{\mu_0}{\pi}\sqrt{r_x r_y}\int_0^{\pi} \frac{\left[1-\frac{c}{r_y}\cos\phi\right]\Psi(k)}{\sqrt{V^3}}d\phi \tag{4.6}$$

4.2.3 Proposed adaptive method

When the receiver is in close proximity enough with the transmitter, the frequency splitting would occur, causing a considerable decrease in the system performance. Figure 4-12 illustrates a theoretical plot of S_{21} parameter as a function of D_1 and D_2, originating from the above circuit derivations with all the mutual couplings being taken into account. As can be seen, when the D_2 between the transmitter and the receiver varies, there would be corresponding changes in an optimum value of D_1 in order for the power transfer efficiency denoted by S_{21} parameter to be maximized.

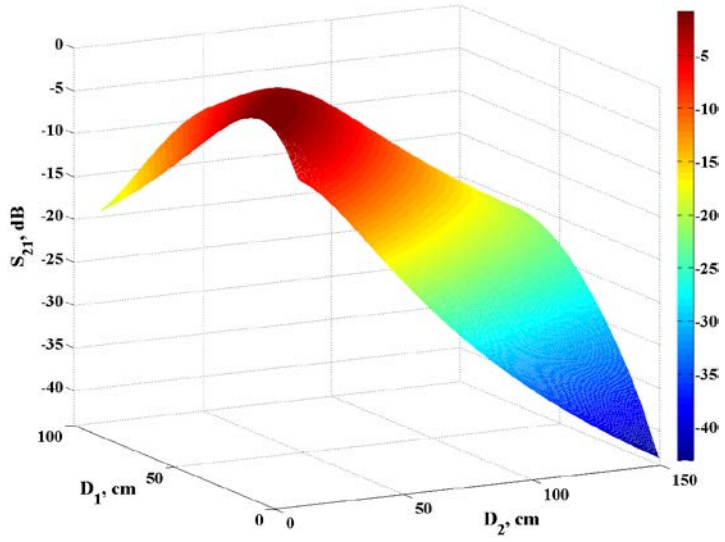

Figure 4-12: S_{21} as a function of D_1 and D_2 (transmitting side: power coil radius = 32 cm, Tx coil radius 35 cm, receiving side: two identical Rx coils radius = 9 cm, two identical load coils radius = 6 cm). The resonant frequency is set at 10 MHz.

Based on that analysis, in this thesis, a novel method of implementing an optimum distance adaptation 'D_1', according to the distance variation between the transmitter and the receivers 'D_2', in the transmitting side enables the system of wireless power transfer to receivers with higher efficiency is proposed.

4.2.4 Results

The above analysis has been verified by Advanced Design System (ADS) and ANSYS HFSS, in addition to experimental implementation. Initially, only one power coil in the transmitting side is used for verification. Figure 4-13 shows an one-turn loop coil with radius of 32 cm and copper wire thickness of 6 mm in an experimental shape (left) and HFSS model (right). The Agilent Technologies 8751A vector network analyzer (VNA) was used to measure the S_{11} parameter of the coil.

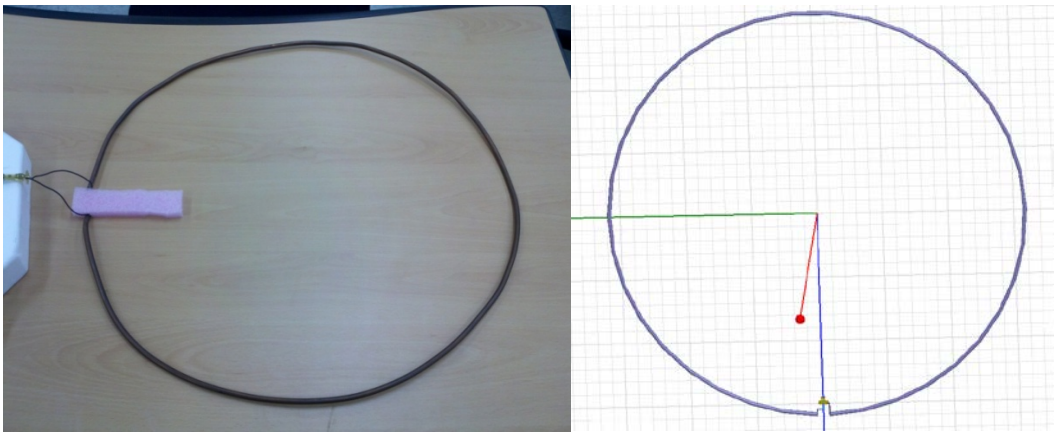

Figure 4-13: One-turn loop coil with radius of 32 cm in experimental shape and HFSS model.

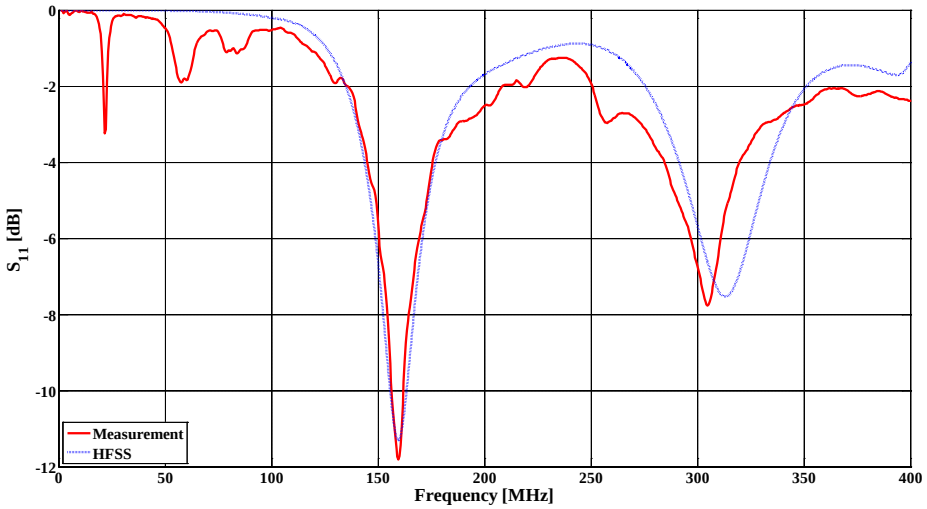

Figure 4-14: Comparison of measured and simulated S_{11} of one-turn loop coil with radius of 32 cm.

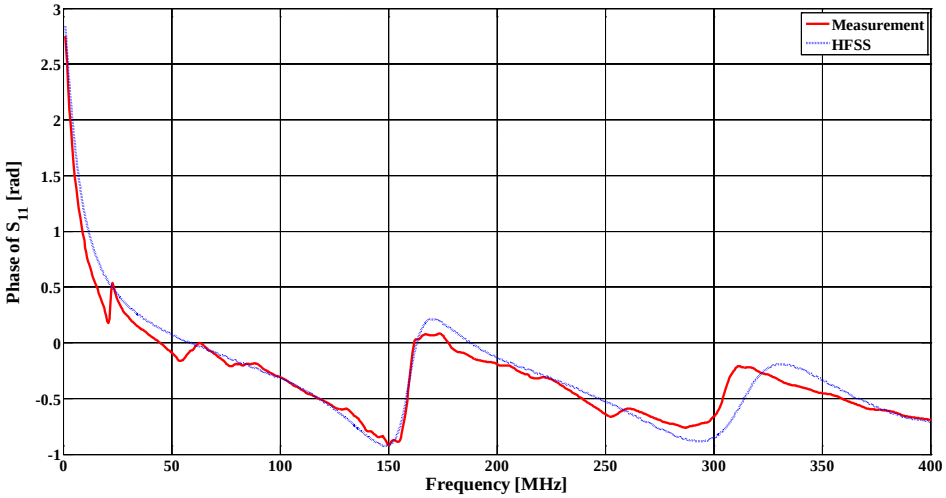

Figure 4-15: Comparison of measured and simulated phase of S_{11} of one-turn loop coil with radius of 32 cm.

Figure 4-14 and 4-15 demonstrate the comparison of the magnitude and phase of S_{11} parameter between experiment and EM simulation in HFSS. It is shown a good agreement between experimental results and results getting from HFSS simulation. Then, the WPT system model in HFSS and its circuit extraction were also verified. The specification of the wireless power transfer system are indicated in Figure 4-16.

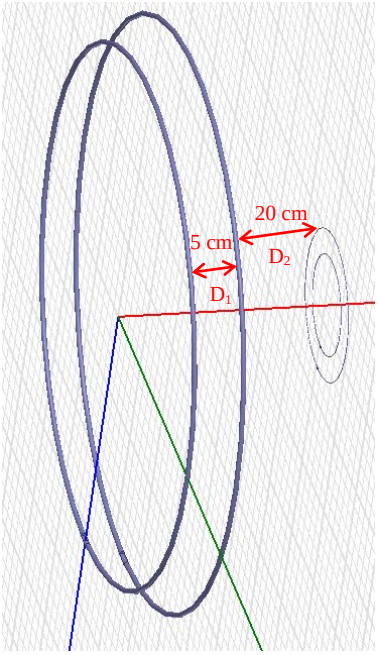

Figure 4-16: WPT system model in HFSS.

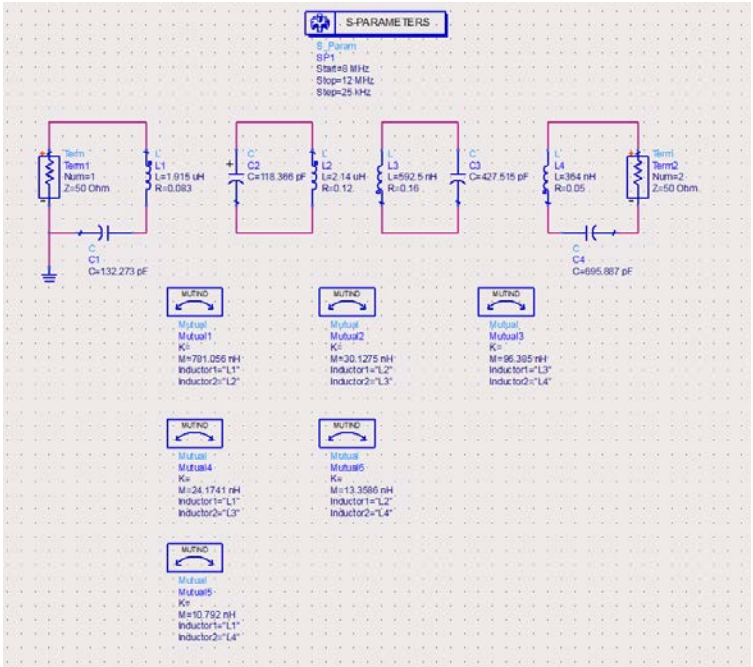

Figure 4-17: Circuit extraction of the above WPT system model in ADS.

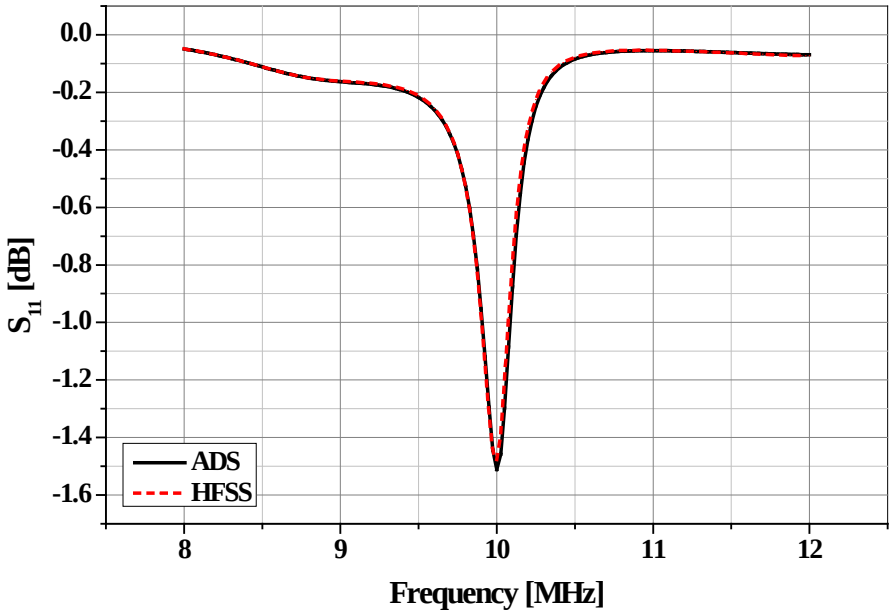

Figure 4-18: S_{11} of the above WPT system model in ADS and HFSS.

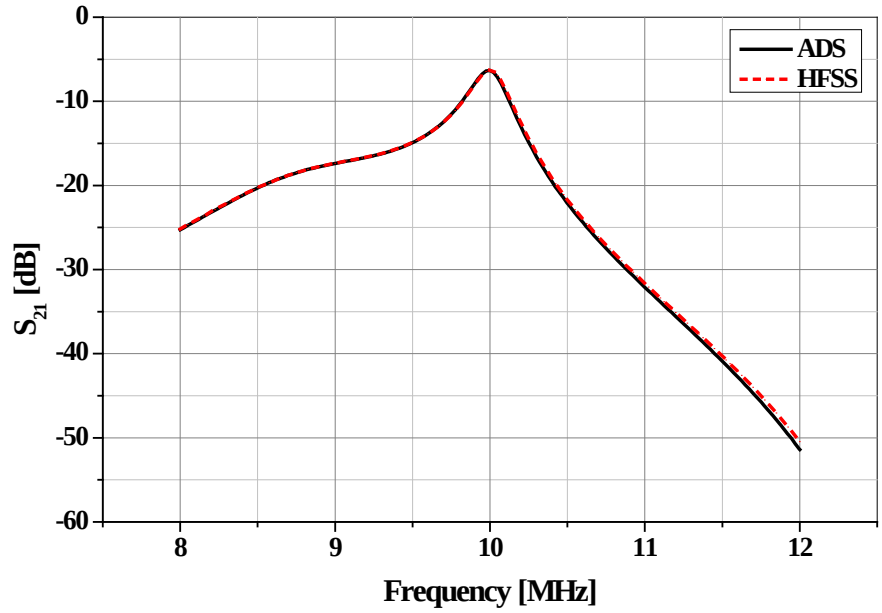

Figure 4-19: S_{21} of the above WPT system model in ADS and HFSS.

The system model in HFSS was shown in figure 4-16 and figure 4-17 shows the circuit extraction of lumped components *R*, *L* and *C* of the above model in ADS. At the distance D_1 of 5 cm and D_2 of 20 cm, the simulated S_{11} and S_{21} parameter by both ADS and HFSS. After the process of the system verification, the proposed method was validated by comparing the WPT system with and without using the adaptive method. The simulation results demonstrated in Figrue 4-20 indicates that the WPT system using the proposed adaptive method achieves higher performance. Additionally, the experimental implementation was also done to verify the effectiveness of the proposed method. The

experimental setup is shown in figure 4-21. All the coils were made of one-turn loops. In the transmitting side, the power coil and Tx coil were with 32 cm and 34 cm of radius, respectively. These two coils were made by 6 mm diameter copper wire.

In the receiving side, the two identical pairs of the Rx and load coils were designed with 10 cm and 5 cm of radius and copper wire thickness of 4 mm. The Rx and load coils of each pair are concentrically located. Variable capacitors were added in the transmitter and receivers to set the resonant frequency of interest. The measured resonant frequency of the implemented system was 10 MHz. The S_{21} parameter was measured by Agilent Technologies 8751A vector network analyzer (VNA) and examined every 5 cm from 15 to 80 cm. The experimental results are plotted in figure 4-21 shows a 11.86 dB boost in S_{21} parameter at the distance D_2 of 80 cm.

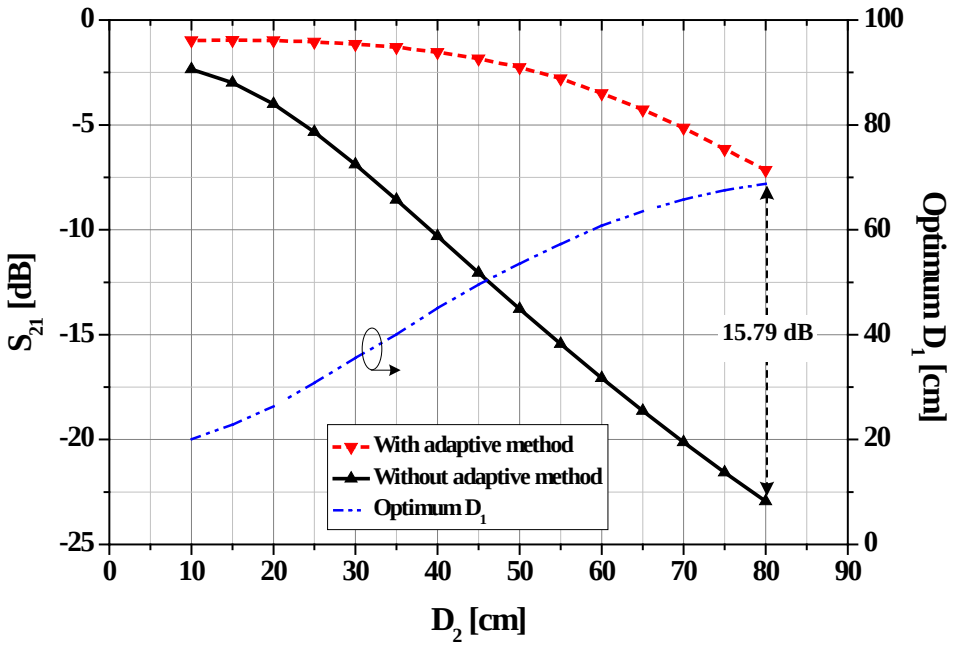

Figure 4-20: Simulated S_{21} parameter comparison between the system with and without the adaptive method. In case of without adaptive method, the D_1 was fixed at 10 cm.

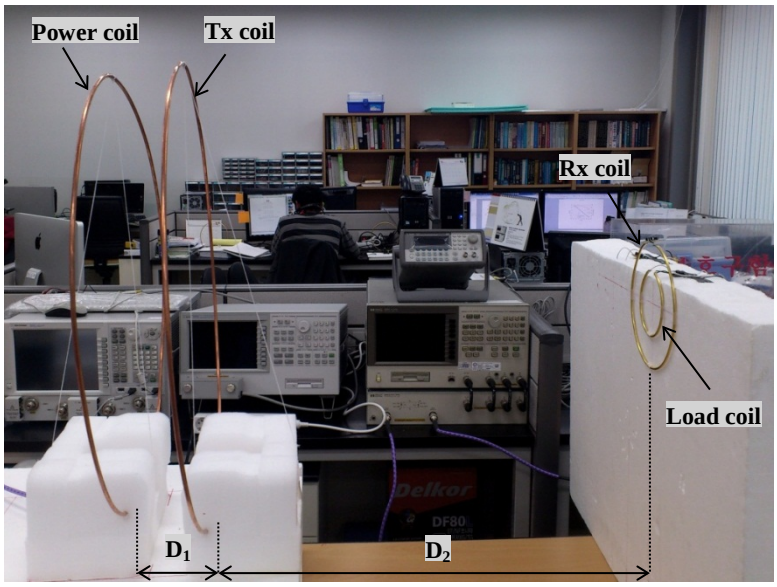

Figure 4-21: Experimental setup of the WPT system with fixed receiver.

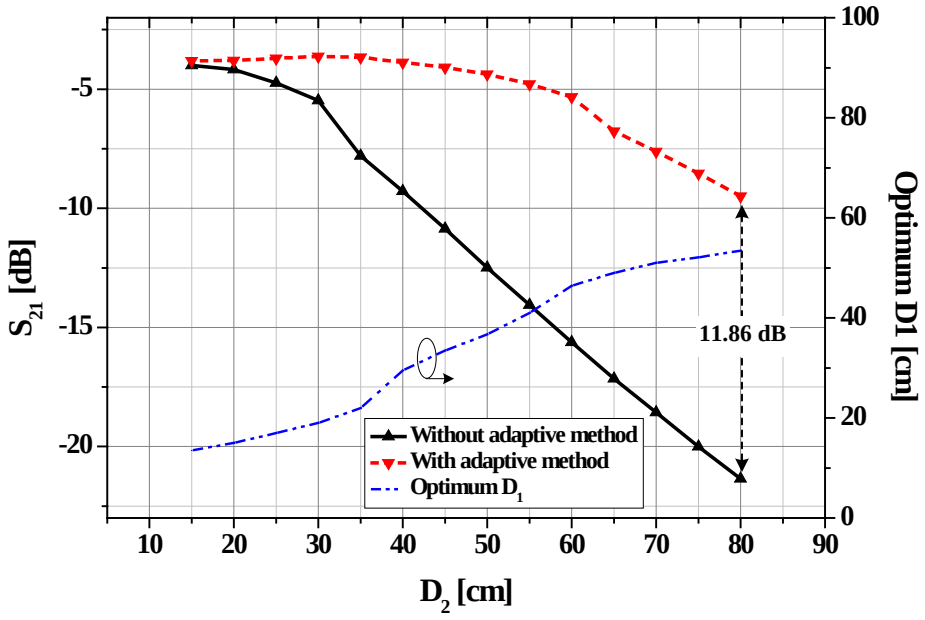

Figure 4-22: Measured S_{21} parameter comparison between the system with and without the adaptive method. In case of without adaptive method, the D_1 was fixed at 10 cm.

4.3 Performance summary

The performances with working conditions of the wireless power transfer systems are summarized in Table 4-1. Various working conditions implemented in these wireless power transfer systems are

demonstrated in this table. The wireless power transfer system in [20] used coils with diameter of 30 cm and 5 turns, while the reference [21] system has 24-cm diameter, 4-turn coils. These system in [20-21] achieved higher efficiency in compared with the system 1 and 2. However, the working distances in [20-21] are much less than the system 1 and 2. Depending on particular applications, the users should choose appropriate system for their designs. For these reasons, Table 4-1 is compared general parameters from measurement.

	[20]	**[21]**	**This work 1**	**This work 2**
Operation Frequency	13.56MHz	27MHz	10.14MHz	10MHz
Distance	20cm	15cm	70cm	80cm
Efficiency	50% (70%)	8% (23%)	39% (51%)	0.5% (10%)

Table 4-1: Comparison with other research results.

Chapter V

Summary & Conclusion

In this thesis, the wireless power transfer system with magnetic resonance was explored from a new perspective and with the enhancement techniques. Firstly, the magnetic resonance based wireless power transfer system was demonstrated using power coil with 49cm diameter and Tx coil that is the helical type with 60cm diameter and 5.25 turns. The symmetric structure is duplicated on the receiving side for the load coil and Rx coil. The experimental results, matched system was shown to confirm the agreement with theoretical predictions, achieving power transfer efficiency of 11.4% improvement at a distance of 70cm and 50% axial-misalignment.

Secondly, the magnetic resonance based wireless power transfer system was constructed using power coil with 64cm diameter, Tx coil with 70cm, Rx coil with 18cm, and load coil with 12cm. According to the theoretical predictions, if coupling coefficient k_{12} is changed in certain distance between transmitter resonator and receiver resonator, coupling coefficient k_{23} could be increased. So the experiment could be achieved power transfer efficiency of approximately 9.5% improvement at a distance of 80cm.

Two adaptive methods were constructed and fully characterized. Using applicable microwave and antenna theory, the lumped parameters were extracted and inserted into a coupled RLC resonator circuit model. The values for impedance matching networks were analytically extracted. Then the impedance matching networks were demonstrated and installed. Experimental results closely agreed with both analytical investigations and simulated results. The benefits of using properly impedance transformation systems were validated by the experimental results.

Finally, this thesis about wireless power transfer with magnetic resonance was not analyzed with the electromagnetic wave theory but with the electrical and radio wave engineering theory to emphasize the essential elements of wireless power transfer with magnetic resonance such as loaded quality factor about resonators, impedance transfer technique, represented equivalent circuit, efficiency enhancement technology. A transmitter and receiver system prototype was developed to verify the theory and to discuss the realizable performance of implemented resonators and impedance transfer circuit. The resonator was a loop and helix with copper wires. It has benefits for demonstration about wireless power transfer system.

REFERENCES

1. Brown, W.C. 1996, 'The History of Wireless Power Transmission', *Solar Energy*, Jan. Vol. 56, No.1, pp. 3-21.

2. Tesla, N. 1900, 'Apparatus for transmission of electrical energy', *US Patent*, May, No.649621.

3. Tesla, N. 1905, 'Art of transmitting electrical energy through the natural mediums', *US patent*, April 1905, No.787412.

4. Kamat, S.P. 2009, 'Energy management architecture for multimedia applications in battery powered devices', *IEEE Transactions on Consumer Electronics*, May, vol.55, No.2, pp. 763-767.

5. Wu, H.H., Covic, G.A., Boys, J.T., Robertson, D.J. 2011, 'A series tuned inductive power transfer pickup with a controllable AC voltage output', *IEEE Transactions on Power Electronics*, Jan, Vol. 26, No.1, pp.98-109.

6. Benford, J. 2008, 'Space applications of high-power microwaves', IEEE Transactions on Plasma Science, June, Vol.36, No.3, pp.569-581.

7. IEEE-SA Standards Board 1999, 'IEEE standard for safety levels with respect to human exposure to radio frequency electromagnetic fields, 3kHz to 300GHz', *IEEE Std*. C95.1.

8. Karalis, A., Joannopoulos, J.D., Soljacic, M. 2008, 'Efficienct wireless non-radiative mid-range energy transfer', *Annals of Physics*, Jan, Vol.323, No.1, pp.34-48.

9. Dickinson, R.M., Brown, W.C. 1975, 'Radiated microwave power transmission system efficiency measurements', Tech. Memo 33-727, Jet Propulsion Lab., Cal. Inst. Technol. Mar. 15.

10. Grover, F.W. 1944, 'The Calculation of the Mutual Inductance of Circular Filaments in Any Desired Positions'. *Proceeding of the IRE*, Vol.32, No.10, pp.620-629.

11. Babic, S.I., Sirois, F., Akyel, C. 2009, 'Validity check of mutual inductance formulars for circular filaments with lateral and angular misalignments', *Progress In Electromagnetics Research M*, Vol.8, pp.15-26.

12. Akyel, C., Babic, S.I., Mahmoudi, M.M. 2009, 'Mutual inductance calculation for non-coaxial circular air coils with parallel axes', *Progress In Electromagnetics Research*, Vol.91, pp.287-301.

13. Sengupta, D.L., Liepa, V.V. 2006. 'Applied Electromagnetics and Electromagnetic Compatibility', John Wiley and Sons, Inc.

14. Sample, A.P., Meyer, D.A., Smith, J.R. 2011, ‘Analysis, Experimental Results, and Range Adaptation of Magnetically Coupled Resonators for Wireless Power Transfer’, *IEEE Transactions on Industrial Electronics*, Vol.58, No.2, pp.544-554.

15. Orfanidis, S.J. 2008 ‘Electromagnetic waves and antennas’, ECE Department Rutgers University, NJ 08854-8058.

16. Garnica, J., Casanova, J., and Lin, J. 2011, ‘High efficiency mid-range wireless power transfer system’, *IEEE MTT-S int. Microw. Syst. Dig.*, June, pp.73-76.

17. Pozar, D.M. 2004, ‘Microwave engineering’, John Wiley and Sons, Inc. 3rd edition.

18. Ishizaki, T., Fukada, D., Awai, I. 2011, ‘A novel concept for 2-dimensional free-access wireless power transfer system using asymmetric coupling resonators with different sizes’, *Microwave Workshop Series on Innovative Wireless Power Transmission: Technologies, Systems, and Applications (IMWS), 2011 IEEE MTT-S International* , pp.243-246.

19. Duong, P.T., Lee, J.W. 2011, ‘Experimental Results of High-Efficiency Resonant Coupling Wireless Power Transfer Using a Variable Coupling Method’, *Microwave and Wireless Components Letters, IEEE* , Vol.21, No.8, pp.442-444.

20. Tech, C.B., Imura, T., Kato, M., Hori, T. 2010, ‘Basic Study of Improving Efficiency of Wireless Power Transfer via Magnetic Resonance Coupling Based on Impedance Matching’, *IEEE International Symposium on Industrial Electronics (ISIE)*, pp.2011-2016.

21. Mazlouman, S.J., Mahanfa, A., Kaminska, B. 2009, ‘Mid-range Wireless Energy Transfer Using Inductive Resonance for Wireless Sensors’, IEEE International Conference on Computer Design, Oct., pp.517-522.

Acknowledgement

First of all, I would like to thank all those who made this thesis possible. First of all, thanks go to my supervisor, Prof. Franklin Bien. His continuously supports, and encouragement enabled me to develop a concentrating of my research.

I would like to express my gratitude to Prof. Jaejoon Kim and Prof. Jaehyouk Choi for giving me advice about my research as a committee. My deep appreciation goes as well to Minh Huy Hoang, my co-researcher in the wireless power transfer research, in addition to Yunho Choi, Sanghyun Hur for their assistance and support for material and emotional.

Also, I greatly thank my lab members, Bien Integrated Circuit Design Laboratory people. They gave me a valuable advice and motivation for my research progress.

Finally, I really appreciate my parents giving me the most valuable support to study so far.